

UC Santa Barbara

UC Santa Barbara Electronic Theses and Dissertations

Title

Mixtures of Intrinsically Disordered Neuronal Protein Tau and Anionic Liposomes Reveal Distinct Anionic Liposome-Tau Complexes Coexisting with Tau Liquid-Liquid Phase Separated Coacervates

Permalink

<https://escholarship.org/uc/item/3cx6b5td>

Author

Jobanputra, Anjali J.

Publication Date

2024

Peer reviewed|Thesis/dissertation

UNIVERSITY OF CALIFORNIA

Santa Barbara

Mixtures of Intrinsically Disordered Neuronal Protein Tau and Anionic Liposomes
Reveal Distinct Anionic Liposome-Tau Complexes Coexisting with Tau Liquid-Liquid
Phase Separated Coacervates

A Thesis submitted in partial satisfaction of the
requirements for the degree Master of Science
in Biochemistry and Molecular Biology

by

Anjali J. Jobanputra

Committee in charge:

Professor Cyrus Safinya, Chair

Professor Stuart Feinstein

Professor Frederick Dahlquist

June 2024

The thesis of Anjali J Jobanputra is approved.

Stuart Feinstein

Frederick Dahlquist

Cyrus Safinya, Committee Chair

June 2024

Mixtures of Intrinsically Disordered Neuronal Protein Tau and Anionic Liposomes
Reveal Distinct Anionic Liposome-Tau Complexes Coexisting with Tau Liquid-Liquid
Phase Separated Coacervates

Copyright © 2024

By

Anjali J. Jobanputra

ACKNOWLEDGEMENTS

I would like to express my deepest appreciate to Cyrus Safinya, my PI and chair of my committee, for his invaluable patience, advice, and continuous support through my time in the Safinya Lab. Also, this endeavor would not have been possible without my Master's Committee, Stu Feinstein and Rick Dahlquist. Their immense knowledge and plentiful experience have encouraged me throughout this journey. I would like to extend my sincere thanks Christine Tchounwou who mentored me as an undergraduate in the lab. Learning from you has shaped me into the scientist that I am today. Many thanks to Youli Li and Kai Ewert for their technical support and feedback on my study.

Special thanks to the RISE program, Department of Energy, Office of Basic Energy Sciences, Division of Materials Sciences and Engineering, and the US National Science Foundation, Division of Materials Research for your generous support along my project. I would also like to thank the BMSE and MCDB department including my advisors Stella Han and Angela Zeng.

I am also grateful for Willus Fisher, Aria Ghasemizadeh, and Bretton Fletcher for their guidance and mentorship in the lab. Finally, words cannot express my gratitude to my family. Their belief in has kept my spirits and motivation high during this process. Last, I would like to thank my friends for the entertainment and emotional support.

ABSTRACT

Mixtures of Intrinsically Disordered Neuronal Protein Tau and Anionic Liposomes Reveal Distinct Anionic Liposome-Tau Complexes Coexisting with Tau Liquid-Liquid Phase Separated Coacervates

by

Anjali J Jobanputra

Microtubules (MTs) are protein nanotubes comprised of $\alpha\beta$ -tubulin heterodimers that act as structural components of the cytoskeleton and carry a net negative charge. Tau, an intrinsically disordered neuronal protein and polyampholyte with an overall positive charge, is a microtubule associated protein, which binds to anionic domains of microtubules (MTs) and suppresses their dynamic instability. Aberrant tau-MT interactions are implicated in Alzheimer's and other neurodegenerative diseases. Here, we studied the interactions between full length human protein tau and other negatively charged binding substrates, as revealed by differential-interference-contrast (DIC) and fluorescence microscopy. As binding substrates we chose anionic liposomes (ALs) containing either 1,2-dioleoyl-sn-glycero-3-phosphatidylserine (DOPS, -1e) or 1,2-dioleoyl-sn-glycero-3-phosphatidylglycerol (DOPG, -1e) mixed with zwitterionic 1,2-dioleoyl-sn-glycero-3-phosphatidylcholine (DOPC) to mimic anionic plasma membranes of axons where tau resides. At low salt concentrations (0 to 10 mM KCl or NaCl) with minimal charge screening, reaction mixtures of tau and ALs resulted

in the formation of distinct states of AL-tau complexes coexisting with liquid-liquid phase separated tau self-coacervates arising from the polyampholytic nature of tau containing cationic and anionic domains. AL-tau complexes exhibited distinct types of morphologies, including, large $\approx 20\text{-}30$ micron giant multi-lamellar liposomes with bound tau-membrane domains and finite-sized assemblies of smaller liposomes glued together through the cationic domains of tau. As the ionic strength of the solution was increased to near and above physiological salt concentrations (≈ 150 mM 1:1 electrolyte), AL-tau complexes remained stable while tau self-coacervate droplets were found to dissolve indicative of breaking of inter- and intra- tau (anionic/cationic) electrostatic bonds due to increased charge screening. The findings are consistent with the hypothesis that cationic domains of tau may interact with anionic domains of the lumen facing lipid monolayer of the axon plasma membranes (where most anionic lipids reside), suggesting the possibility of transient yet robust interactions at physiologically relevant ionic strengths.

TABLE OF CONTENTS

I. Introduction.....1-5

II. Methods.....6-9

 A. Tau Purification.....6-7

 B. Tau Labeling.....7

 C. Liposome Preparation.....7-8

 D. DIC Microscopy.....8-9

 E. Fluorescence Microscopy.....9

III. Results and Discussion.....10-28

 A. Salt-Dependent Behavior of 4RL Tau Self-Coacervates.....10-11

 B. Anionic Liposomes at Low and High Salt Concentrations.....12-13

 C. Phase Separated States in Mixtures of Anionic Liposomes and Tau in Deionized
Water.....14-18

 D. Comparison of Phase Separated States in Mixtures of Anionic Liposomes and Tau
in Low versus High Salt.....19-20

 E. Mixture of Anionic Liposomes and Tau in Low Salt21-23

 F. Mixture of Anionic Liposomes and Tau in High Salt24-29

IV. Conclusion.....30-31

References.....32-35

Appendix.....36

LIST OF FIGURES

- Figure 1. **Illustration of tau binding to a microtubule and charge distribution of the full-length 4RL isoform of tau used in the study.** (a) Tau binds to the surface of MT (red/blue) at the MTBR (yellow). The PD (green/purple) and C-terminal tail (grey/teal) extend of the surface of the microtubule. (b) Charge distribution (averaged over 10 residues) of the primary sequence of 4RL tau (anionic character in dark blue, cationic character in dark grey). Below, alternative splicing of exons 2 (red-rectangle), 3 (orange), and 10 (blue) result in the five additional wild-type isoforms of tau. Each isoform contains NTT (PD – green/purple background, PRR – grey), MTBR (yellow), and CCT (grey/teal). Figure adapted from Chung et al²¹..... 1
- Figure 2. **Electrostatic interactions of tau coacervates break near physiological salt concentration.** (a) Cartoon of 4RL undergoing intermolecular electrostatic interactions to create a tau coacervate in deionized water. (b-f) Differential interference contrast (DIC) microscopy images of full length 4RL tau tagged with Alexa-546 in increasing KCl concentrations (0-300mM). (g-k) Fluorescent microscopy of full length 4RL tau tagged with Alexa-546 visible in the RFP channel (Alexa 546 excitation/emission: 561nm/572nm) in increasing KCl concentrations (0-300mM). (l-n) Zoomed-in inset of corresponding DIC images linked by dashed line scaled by a factor of 2. All scale bars = 50 μ m. 12
- Figure 3. **Observation of anionic liposomes at low and high salt conditions.** (a) Chemical structures of DOPS (C18:1, Q = -1), DOPG (C18:1, Q = -1), DOPC (C18:1, zwitterion) and Cy5.5-PE (C18:1) lipids used to make anionic liposomes for experiments. (b-d) DIC microscopy images of unsonicated anionic liposomes tagged with Cy5.5-PE (50% DOPS/ 49%DOPC/1% CY5.5 PE) in increasing KCl concentrations (10-300mM). (e-g) Fluorescent microscopy of unsonicated anionic liposomes tagged with Cy5.5-PE (50% DOPS/ 49%DOPC/1% CY5.5 PE) visible in the Cy5 channel (Cy5.5 PE lipid - excitation/emission 683nm/703nm) in increasing KCl concentrations (10-300mM). (h-j) Zoomed-in inset of corresponding DIC images linked by dashed line scaled by a factor of 2. All scale bars = 50 μ m..... 13
- Figure 4. **Fluorescent microscopy images of anionic liposomes made of 50% DOPG/ 49%DOPC/1% CY5.5 PE interacting with 4RL tau in deionized water.** The lipid channel (Cy5) is shown in RED (excitation/emission 683nm/703nm) and 4RL tau tagged with Alexa-488, is shown in the GFP channel (GREEN) (excitation/emission: 488nm/496nm). (a) A 3D Z-stack image series showing both GFP and Cy5 channels. The main image frame (top left panel) shows the X-Y section view at a chosen Z. The projection to the right shows the Y-Z side views slicing along the vertical dotted lines of three circles objects. The bottom panel shows the X-Z slices along the horizontal dotted lines. The X-Z and Y-Z plane side views of each circled object are indicated by the end of the dotted lines in each direction. (Scale bars correspond to 50 μ m in the X-Y plane, 200 μ m in X-Z and 20 μ m in Y-Z planes, respectively) (b) Detail view of particle 1: a giant liposome-4RL tau complex. Top panel from left to right: magnified

fluorescent (Cy5, GFP and GFP/Cy5 overlay) and DIC images of particle 1. Bottom panel: fluorescent intensity profiles of particle 1 in Cy5/GFP channels as a function of X. (c) Detail view of particle 2: an anionic liposome-4RL tau complex shown in magnified fluorescent (Cy5, GFP and GFP/Cy5 overlay) and DIC images, and fluorescent intensity traces as a function of X. (d) Detail view of particle 3: a tau coacervate with lipid assembly shown in magnified fluorescent (Cy5, GFP and GFP/Cy5 overlay) and DIC images, and fluorescent intensity traces as a function of X. Scales bar in (b-d) = 10 μ m.17

Figure 5. Fluorescent microscopy images of anionic liposomes made of 50% DOPS/49% DOPC/1% CY5.5 PE and 4RL tau in deionized water. The lipid channel is shown in the RED Cy5 channel (excitation/emission 683nm/703nm) and 4RL tau tagged with Alexa-488 is shown in GREEN in the GFP channel (excitation/emission: 488nm/496nm). (a) A Z-stack image series showing both GFP and Cy5 channels. The top left frame shows the X-Y plane view at a chosen Z. The three panels to the right show the Y-Z slices along vertical dotted lines marking three circles objects 1-3. The bottom panels are the X-Z side views (slices) along the horizontal dotted lines of circles objects 1-3. The Z-X and Y-Z plane side views of each circled object are indicated by the end of the dotted lines in each direction. (Scale bars correspond to 50 μ m in the X-Y, 200 μ m in X-Z and 20 μ m in Y-Z planes, respectively) (b) Detail view of particle 1: a giant liposome-4RL tau complex. Top panel from left to right: magnified fluorescent (Cy5, GFP and GFP/Cy5 overlay) and DIC images of particle 1. Bottom panel: fluorescent intensity profiles of particle 1 in Cy5/GFP channels as a function of X. (c) Detail view of particle 2: an anionic liposome-4RL tau complex shown in magnified fluorescent (Cy5, GFP and GFP/Cy5 overlay) and DIC images, and fluorescent intensity traces as a function of X. (d) Detail view of particle 3: a tau coacervate with lipid assembly shown in magnified fluorescent (Cy5, GFP and GFP/Cy5 overlay) and DIC images, and fluorescent intensity traces as a function of X. Scales bar in (b-d) = 10 μ m.18

Figure 6. Electrostatic interactions in tau coacervates are weaker than anionic liposome-tau interactions. (a, b) DIC microscopy images of full length 4RL tau tagged with Alexa-546 and unlabeled anionic lipids (50 mol% DOPG/ 50 mol% DOPC) in low (5mM) and high (150mM) KCl concentrations. (c, d) fluorescent microscopy images in the RFP channel corresponding to (a,b) showing full length 4RL tau tagged with Alexa-546 (excitation/emission: 561nm/572nm). [50 μ m scale bar] (e, f) DIC microscopy images of full length 4RL tau tagged with Alexa-546 and unlabeled anionic lipids (50 mol% DOPG/ 50 mol% DOPC) in low (5mM) and high (150mM) NaCl concentrations. (g, h) RFP fluorescent images corresponding to DIC images shown in (e, f). [50 μ m scale bar].....20

Figure 7. Fluorescent microscopy images of anionic liposomes and 4RL tau in 10mM KCl. The anionic liposomes made from 50% DOPS/ 49% DOPC/1% CY5.5 PE are visible in the Cy5 channel (RED) (Cy5.5 PE lipid - excitation/emission 683nm/703nm) and 4RL tau tagged with Alexa-488 (Alexa 488 excitation/emission: 488nm/496nm)

are visible in the GFP channel (green). (a) A Z-stack image showing both GFP and Cy5 channels. The top left frame shows the X-Y section view at a chosen Z. The panels to the right show the Y-Z slice along the vertical dotted line marking the circled object 1. The bottom panel shows the X-Z section along the horizontal dotted line of object 1. (Scale bars correspond to 50 μ m in the X-Y, 200 μ m in X-Z and 20 μ m in Y-Z planes, respectively) (b) Detail view of particle 1: a giant anionic liposome-4RL tau complex. Top panel from left to right: magnified fluorescent (Cy5, GFP and GFP/Cy5 overlay) and DIC images of particle 1. Bottom panel: fluorescent intensity profiles of particle 1 in Cy5/GFP channels as a function of X. [10 μ m scale bars].....21

Figure 8. **Fluorescent microscopy images of anionic liposomes and 4RL tau in 10mM KCl.** The anionic liposomes made from 50% DOPS/ 49%DOPC/1% CY5.5 PE are visible in the Cy5 channel (RED) (Cy5.5 PE lipid - excitation/emission 683nm/703nm) and 4RL tau tagged with Alexa-488 (Alexa 488 excitation/emission: 488nm/496nm) are visible in the GFP channel (green). (a) A Z-stack image showing both GFP and Cy5 channels. The top left frame shows the X-Y section view at a chosen Z. The panels to the right show the Y-Z slice along the vertical dotted line marking the circled object 2. The bottom panel shows the X-Z section along the horizontal dotted line of object 2. (Scale bars correspond to 50 μ m in the X-Y, 200 μ m in X-Z and 20 μ m in Y-Z planes, respectively) (b) Detail view of particle 2: a anionic liposome-4RL tau complex. Top panel from left to right: magnified fluorescent (Cy5, GFP and GFP/Cy5 overlay) and DIC images of particle 2. Bottom panel: fluorescent intensity profiles of particle 2 in Cy5/GFP channels as a function of X. [10 μ m scale bars].....22

Figure 9. **Fluorescent microscopy images of anionic liposomes and 4RL tau in 10mM KCl.** The anionic liposomes made from 50% DOPS/ 49%DOPC/1% CY5.5 PE are visible in the Cy5 channel (RED) (Cy5.5 PE lipid - excitation/emission 683nm/703nm) and 4RL tau tagged with Alexa-488 (Alexa 488 excitation/emission: 488nm/496nm) are visible in the GFP channel (green). (a) A Z-stack image showing both GFP and Cy5 channels. The top left frame shows the X-Y section view at a chosen Z. The panels to the right show the Y-Z slice along the vertical dotted line marking the circled object 3. The bottom panel shows the X-Z section along the horizontal dotted line of object 3. (Scale bars correspond to 50 μ m in the X-Y, 200 μ m in X-Z and 20 μ m in Y-Z planes, respectively) (b) Detail view of particle 3: a tau coacervate. Top panel from left to right: magnified fluorescent (Cy5, GFP and GFP/Cy5 overlay) and DIC images of particle 3. Bottom panel: fluorescent intensity profiles of particle 3 in Cy5/GFP channels as a function of X. [10 μ m scale bars].....23

Figure 10. **Fluorescent microscopy images of anionic liposomes and 4RL tau in 100mM KCl.** The anionic liposomes made from 50% DOPS/ 49%DOPC/1% CY5.5 PE are visible in the Cy5 channel (RED) (Cy5.5 PE lipid - excitation/emission 683nm/703nm) and 4RL tau tagged with Alexa-488 (Alexa 488 excitation/emission: 488nm/496nm) are visible in the GFP channel (green). (a) A Z-stack image showing both GFP and Cy5 channels. The top left frame shows the X-Y section view at a chosen Z. The panels

to the right show the Y-Z slice along the vertical dotted line marking the circled object 1. The bottom panel shows the X-Z section along the horizontal dotted line of object 1. (Scale bars correspond to 50 μ m in the X-Y, 200 μ m in X-Z and 20 μ m in Y-Z planes, respectively) (b) Detail view of particle 1: a giant anionic liposome-4RL tau complex. Top panel from left to right: magnified fluorescent (Cy5, GFP and GFP/Cy5 overlay) and DIC images of particle 1. Bottom panel: fluorescent intensity profiles of particle 1 in Cy5/GFP channels as a function of X. [10 μ m scale bars]25

Figure 11. **Fluorescent microscopy images of anionic liposomes and 4RL tau in 10mM KCl.** The anionic liposomes made from 50% DOPS/ 49%DOPC/1% CY5.5 PE are visible in the Cy5 channel (RED) (Cy5.5 PE lipid - excitation/emission 683nm/703nm) and 4RL tau tagged with Alexa-488 (Alexa 488 excitation/emission: 488nm/496nm) are visible in the GFP channel (green). (a) A Z-stack image showing both GFP and Cy5 channels. The top left frame shows the X-Y section view at a chosen Z. The panels to the right show the Y-Z slice along the vertical dotted line marking the circled object 2. The bottom panel shows the X-Z section along the horizontal dotted line of object 2. (Scale bars correspond to 50 μ m in the X-Y, 200 μ m in X-Z and 20 μ m in Y-Z planes, respectively) (b) Detail view of particle 2: a anionic liposome-4RL tau complex. Top panel from left to right: magnified fluorescent (Cy5, GFP and GFP/Cy5 overlay) and DIC images of particle 2. Bottom panel: fluorescent intensity profiles of particle 2 in Cy5/GFP channels as a function of X. [10 μ m scale bars]26

Figure 12. **Fluorescent microscopy images of anionic liposomes and 4RL tau in 150mM KCl.** The anionic liposomes made from 50% DOPS/ 49%DOPC/1% CY5.5 PE are visible in the Cy5 channel (RED) (Cy5.5 PE lipid - excitation/emission 683nm/703nm) and 4RL tau tagged with Alexa-488 (Alexa 488 excitation/emission: 488nm/496nm) are visible in the GFP channel (green). (a) A Z-stack image showing both GFP and Cy5 channels. The top left frame shows the X-Y section view at a chosen Z. The panels to the right show the Y-Z slice along the vertical dotted line marking the circled object 1. The bottom panel shows the X-Z section along the horizontal dotted line of object 1. (Scale bars correspond to 50 μ m in the X-Y, 200 μ m in X-Z and 20 μ m in Y-Z planes, respectively) (b) Detail view of particle 1: a giant anionic liposome-4RL tau complex. Top panel from left to right: magnified fluorescent (Cy5, GFP and GFP/Cy5 overlay) and DIC images of particle 1. Bottom panel: fluorescent intensity profiles of particle 1 in Cy5/GFP channels as a function of X. [10 μ m scale bars]27

Figure 13. **Fluorescent microscopy images of anionic liposomes and 4RL tau in 150mM KCl.** The anionic liposomes made from 50% DOPS/ 49%DOPC/1% CY5.5 PE are visible in the Cy5 channel (RED) (Cy5.5 PE lipid - excitation/emission 683nm/703nm) and 4RL tau tagged with Alexa-488 (Alexa 488 excitation/emission: 488nm/496nm) are visible in the GFP channel (green). (a) A Z-stack image showing both GFP and Cy5 channels. The top left frame shows the X-Y section view at a chosen Z. The panels to the right show the Y-Z slice along the vertical dotted line marking the circled object

2. The bottom panel shows the X-Z section along the horizontal dotted line of object 2. (Scale bars correspond to 50 μ m in the X-Y, 200 μ m in X-Z and 20 μ m in Y-Z planes, respectively) (b) Detail view of particle 2: a anionic liposome-4RL tau complex. Top panel from left to right: magnified fluorescent (Cy5, GFP and GFP/Cy5 overlay) and DIC images of particle 2. Bottom panel: fluorescent intensity profiles of particle 2 in Cy5/GFP channels as a function of X. [10 μ m scale bars]28

Figure 14. **Fluorescent microscopy images of anionic liposomes and 4RL tau in 150mM KCl.** The anionic liposomes made from 50% DOPS/ 49%DOPC/1% CY5.5 PE are visible in the Cy5 channel (RED) (Cy5.5 PE lipid - excitation/emission 683nm/703nm) and 4RL tau tagged with Alexa-488 (Alexa 488 excitation/emission: 488nm/496nm) are visible in the GFP channel (green). (a) A Z-stack image showing both GFP and Cy5 channels. The top left frame shows the X-Y section view at a chosen Z. The panels to the right show the Y-Z slice along the vertical dotted line marking the circled object 3. The bottom panel shows the X-Z section along the horizontal dotted line of object 3. (Scale bars correspond to 50 μ m in the X-Y, 200 μ m in X-Z and 20 μ m in Y-Z planes, respectively) (b) Detail view of particle 3: a tau coacervate with lipid assembly. Top panel from left to right: magnified fluorescent (Cy5, GFP and GFP/Cy5 overlay) and DIC images of particle 3. Bottom panel: fluorescent intensity profiles of particle 3 in Cy5/GFP channels as a function of X. [10 μ m scale bars]28

Appendix Figure 1. **Coacervate with hints of lipid assembly produced in mixture of anionic liposomes (50% DOPS/ 49%DOPC/1% CY5.5 PE) and 4RL tau tagged with Alexa-488 in 150mM KCl.** (1-5) Slice taken of coacervate of merged CY5/GFP channel. (Cy5.5 PE lipid - excitation/emission 683nm/703nm) (Alexa 488 excitation/emission: 488nm/496nm). (a-e) 3D intensity maps taken at slice shown on particle.....36

I. Introduction

Human tau is an intrinsically disordered protein (IDP). It is an overall positive polyampholyte (i.e. containing positive and negative residues) with six wild-type central nervous system (CNS) isoforms.¹ Tau's N-terminal tail (NTT) is made up of a projection domain (PD) and proline rich region (PRR) (Fig. 1a). This is followed by the microtubule binding region (MTBR) and a carboxyl-terminal tail (CTT). Alternative splicing of exons 2, 3, and 10 of the tau gene results in the six CNS isoforms (Fig. 1a).^{2,3,4,5} The prevailing model is that tau binds the carboxyl-terminal tail of α -tubulin at positive MTBR and possibly PRR regions enriched in positive residues (Fig. 1b).^{3,4,5,6} In our study we used the full-length isoform (4RL-tau).

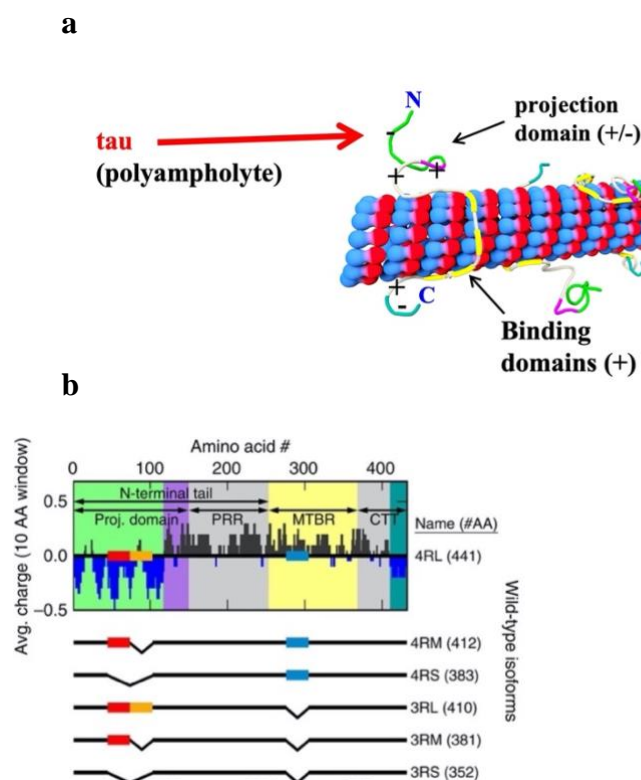


Figure 1. Illustration of tau binding to a microtubule and charge distribution of the full-length 4RL isoform of tau used in the study. (a) Tau binds to the surface of MT (red/blue) at the MTBR (yellow). The PD (green/purple) and C-terminal tail (grey/teal)

extend of the surface of the microtubule. (b) Charge distribution (averaged over 10 residues) of the primary sequence of 4RL tau (anionic character in dark blue, cationic character in dark grey). Below, alternative splicing of exons 2 (red-rectangle), 3 (orange), and 10 (blue) result in the five additional wild-type isoforms of tau. Each isoform contains NTT (PD – green/purple background, PRR – grey), MTBR (yellow), and CCT (grey/teal). Figure adapted from Chung et al²¹.

Tau is a microtubule-associate protein (MAP) that is confined primarily to the axonal compartment in mature neurons. Microtubules (MTs) are components of the cytoskeleton found in eukaryotes and are made up of $\alpha\beta$ -tubulin heterodimers with a net negative charge that self-organize into hollow nanotubes containing protofilaments (i.e. oligomers of $\alpha\beta$ -tubulin) (Fig. 1b).^{7,8,9,10} MTs, in association with MAPs and other cellular proteins, play an important role in cell motility, establishing cell shape, intracellular trafficking, and chromosome segregation.^{11,12} Bare MTs are highly dynamic and stochastically switch between cycles of slow growth (polymerization) and rapid shrinkage (depolymerization) known as dynamical instability (DI).^{11,13,14,15,16,17}

While IDP Tau's natural substrate is $\alpha\beta$ -tubulin, it further has distinct roles in neurons many of which are not fully understood.^{1,2,3,4,5,6,18,19,20,21,22} In developing neurons, tau is associated with axon establishment and elongation, while in mature neurons, tau binds and stabilizes microtubules by suppressing dynamic instability (Figure 1a).^{11,23,24,25,26,27,28} This stabilization allows for proper trafficking of organelles along MT in axons, a process known as axonal transport. However tau dysfunction, thought to occur via hyperphosphorylation, leads to dissociation of tau from MT binding sites.²⁹ The excess soluble tau forms phase separated fibers and tangles of fibers most likely driven by interactions with oppositely charged macromolecules such as RNA. These tau tangles are known as neurofibrillary tangles

and are very common in patients with Alzheimer's Disease, Frontotemporal Dementia and Parkinsonism (FTDP-17) and several other dementia diseases.^{30,31}

The experimental study described here was designed in order to identify interactions between full length 4RL-tau (Fig. 1b) and other biologically relevant negatively charged binding substrates. A potential substrate for tau, in addition to tau's natural substrate, namely, net negative $\alpha\beta$ -tubulin whether in the MT lattice or not, may be the plasma membrane of axons where lipids with negative charge headgroups (e.g. phosphatidylserine or phosphatidylinositol-4,5 biphosphate) reside in the inner layer, facing the axonal cytosol.^{32,33,34} To model the negative plasma membrane, anionic liposomes were prepared and their reaction mixtures with 4RL-tau were investigated for identification of phase separated states resulting from the electrostatic interactions. The initial studies involved tau-alone control experiments using 4RL-tau tagged with Alexa-546, visible in the RFP channel, in varying salt concentrations of KCl or NaCl, using both differential-interference-contrast (DIC) and fluorescence microscopy. Liquid-liquid phase separated tau self-coacervates were observed at low ionic strength, arising from the polyampholytic nature of tau containing cationic and anionic domains and leading to attractive electrostatic interactions.³⁵ The tau self-coacervates were observed to significantly weaken and effectively dissolve with increasing ionic strength. This is consistent with earlier observations that tau coacervates can only retain their stability at these high ionic strengths by the addition of a depletant resulting in osmotic crowding.^{36,37} Tau coacervates have been hypothesized to potentially be a precursor state to the neurofibrillary tangles in neurodegeneration.^{35,38}

Similarly, the anionic liposome samples (with no added tau) consisting of zwitterionic 1,2-dioleoyl-sn-glycero-3-phosphatidylcholine (DOPC, charge = 0) mixed with either 1,2-

dioleoyl-sn-glycero-3-phospho-L-serine (DOPS, charge = -1e) or 1,2-dioleoyl-sn-glycero-3-phospho-(1'-rac-glycerol) (DOPG, charge = -1e) and tagged with Cy5.5PE visible in the Cy5 Channel, exhibited morphologies (including giant multi-lamellar liposomes and small uni- and multi-lamellar vesicles), over the range of ionic strengths studied (0 mM to 300 mM, 1:1 electrolytes).¹¹

We conducted optical imaging experiments of reaction mixtures of the labeled tau and anionic liposomes (ALs) in varying salt concentrations using DIC and fluorescence microscopy to elucidate the new phase separated states occurring in the reaction mixtures. Experiments with both the anionic liposomes unlabeled (50% DOPS/ 50%DOPC) or (50% DOPG/ 50%DOPC) and labeled (50% DOPS/ 49%DOPC/1% CY5.5 PE) or (50% DOPG/ 49%DOPC/1% CY5.5 PE) were performed with the labeled tau. Intensity scans were taken of the various types of particles produced.

Distinct phase separated states were formed in the low salt concentration regime in mixtures with no added salt and with 10 mM KCl or NaCl. A large fraction of the sample, consisting of reaction mixtures of tau and ALs, resulted in the formation of AL-tau complexes. The distinct complex morphologies included giant uni- and multi-lamellar vesicles with bound tau-membrane domains (i.e. similar to colloidal nanoparticles bound to giant vesicles) and finite-sized assemblies of small liposomes glued together through the cationic domains of tau.³⁹ The tau-mediated assemblies of small liposomes exhibited morphologies similar to vesosomes where for the latter system, the liposome assembly is achieved through encapsulation inside a larger unilamellar liposomal compartment.^{40,41}

A separate distinct state coexisting with AL-tau complexes (or tau-lipoplexes) was the liquid-liquid phase separated tau coacervate, which appeared to contain little to no lipid.

Significantly, as a function of increasing NaCl or KCl concentrations from 0 to 300 mM, the AL-tau complexes remained stable, while the tau coacervate droplets were found to rapidly dissolve as the ionic strength approached physiological salt conditions ($\approx 150\text{mM}$ 1:1 electrolyte). This behavior for tau coacervates suggests that the breaking of inter- and intra-tau (anionic/cationic) electrostatic bonds is due to the increased charge screening with increasing salt concentrations. These findings raise the possibility that the cationic domains of tau, either bound to MTs or upon unbinding from MTs, may form stable transient bonds with anionic domains of the inner layer of axonal plasma membranes.

It is interesting to point out that AL-tau complexes (or tau-lipoplexes), are analogous to well-known lipoplexes, consisting of complexes of cationic liposomes (CLs) and oppositely charged nucleic acids, used in delivery applications.^{43,44,45,46,47} CL-DNA and CL-siRNA lipoplexes exhibit distinct structures as revealed by synchrotron small-angle X-ray scattering. These include, the lamellar L_{α}^C phase and PEGylated lamellar lipoplex nanoparticles with alternating lipid bilayers and DNA monolayers, inverted hexagonal H_{II}^C and hexagonal H_I^C phases with DNA inserted in inverse cylindrical micelles or surrounded by cylindrical micelles, respectively.^{48,49,50,51,52,53,54} For short double stranded siRNA, CL-siRNA complexes may further form gyroid cubic phase ($Q_{II}^{G, siRNA}$) structures where the siRNA is in the two water channels.^{55,56} The structures of recently developed mRNA-lipid nanoparticles (LNPs) used in vaccines, similarly reveal a disordered inverse hexagonal H_{II}^c and cubic phases.^{57,58}

II. Methods

A. *Tau Purification*

The expression vector (pRK172) encoding full-length (4RL) tau with ampicillin resistance was gifted by Dr. Kenneth Kosik (University of California, Santa Barbara). Tau plasmids were transformed into BL21(DE3) competent cells and streaked on Luria broth agar (5g tryptone, 2.5g yeast extract, and 5g NaCl in DI water) plates containing 0.1% ampicillin before a ~14hr incubation at 37°C. A single colony was inoculated in 250 mL of Luria broth overnight (18hr) at 37°C followed by a 24h incubation in 6L of auto-induction media (10g tryptone, 5g yeast extract, 0.5g dextrose, 2g α -D-lactose, and 5 mL of glycerol per liter of DI water with 25mM NaHPO₄, 25mM KH₂PO₄, 50mM NH₄Cl, 5mM Na₂SO₄ dissolved). Bacteria were harvested for lysis by centrifugation (5,000rpm for 15min in GS-3 Rotor) in a Sorvall RC-5B Plus centrifuge held between 4 to 10 °C. Pelleted bacteria were resuspended in BRB80 buffer (80mM PIPES, 1mM EGTA and 1mM MgSO₄) pH 6.8 which includes ~120mM NaOH (to obtain the correct pH) as well as 0.1% β ME and 0.5% AEBSF (a protease inhibitor). Following, cells were lysed in a pressurized French press cell three times at 1200 PSI, boiled and cooled for 10 min each, and centrifuged at 13,000rpm in a SS-34 Rotor for 40 min to pellet the cell debris. The supernatant was collected and passed through a phosphocellulose (P11, Whatman) ion-exchange column to initiate isolation of tau by increasing concentrations of (NH₄)₂SO₄ (50mM, 150mM, and 250mM) in BRB80 for elution. The tau fractions, confirmed by SDS-PAGE, were pooled and the buffer concentration of (NH₄)₂SO₄ increased to 1.25M. The sample was then passed through a hydrophobic interaction chromatography column (HisTrap Phenyl HP, GE Healthcare) and washed with decreasing concentrations (high salt - 1.1M, low salt - 50mM) of (NH₄)₂SO₄ in

BRB80 to elute tau. Tau containing fractions were identified again through SDS-PAGE, pooled, concentrated, and buffer exchanged to fresh BRB80 without $(\text{NH}_4)_2\text{SO}_4$ using an Amicon Ultra-15 Centrifugal Filter with MWCO = 10,000 (EMD Millipore, Darmstadt, Germany) and successive 40min centrifugation cycles at 4,000 rpm. Purified tau stocks were stored at $-80\text{ }^\circ\text{C}$ until needed for experiments. The concentration of tau was determined by SDS-PAGE slope comparison with a tau mass spectrometry standard.

B. Tau Labeling

To attach a fluorophore to purified tau stocks, tau's concentration was confirmed between 50-100 μM in BRB80 (pH ~ 7.0) and thawed in 100-500 μL batches. Next a 10-molar excess of βME is added and the solution is left to sit for 30 minutes at room temperature to reduce tau's disulfide bonds. βME is dialyzed away using a Zeba Spin desalting column (MWCO 7,000, Thermo Fisher Scientific). A 1-10mM stock solution of the dye is then made followed by adding the dye to the tau solution dropwise. In this case, Alexa Fluor-488 C5 maleimide or Alexa Fluor-546 C5 maleimide (Thermo Fisher Scientific) was added depending on experimental parameters. After two hours at room temperature, a 10-molar excess of βME is added and a gel filtration column (Sephadex G-25 Column, Sigma Aldrich) is performed in BRB80 to separate the conjugate. Labeled tau was then stored at $-80\text{ }^\circ\text{C}$ until experimental use.

C. Liposome Preparation

In a small glass vial, stock solutions of each lipid component stored in chloroform purchased from Avanti Polar Lipids, Inc were mixed in chloroform:methanol (3:1, v/v) at a

total molar concentration dependent on the charge ratio (ρ) of lipid/tau =1. For the experiments outlined, liposomes were formulated with lipids of negative charge, 1,2-dioleoyl-sn-glycero-3-phosphatidylserine (DOPS, -1e) or 1,2-dioleoyl-sn-glycero-3-phosphatidylglycerol (DOPG, -1e), mixed with zwitterionic lipids, 1,2-dioleoyl-sn-glycero-3-phosphatidylcholine (DOPC) and some with the fluorophore 1,2-dioleoyl-sn-glycero-3-phosphoethanolamine-N-(Cyanine 5.5) as well. The ratios were based on the final desired concentration and molar composition of each lipid. Liposomes of various molar ratios were formulated including (50% DOPS/ 50%DOPC), (50% DOPG/ 50%DOPC), (50% DOPS/ 49%DOPC/1% CY5.5 PE), and (50% DOPG/ 49%DOPC/1% CY5.5 PE). Lipid mixtures in chloroform:methanol were exposed to a steady stream of nitrogen for 10 min to evaporate the organic solvent and then further dried overnight in a vacuum (rotary vane pump). Dehydrated lipid films were then rehydrated with high-resistivity water (18.2 M Ω cm) determined by the final desired concentration and incubated overnight at 37 °C to form unsonicated liposomes. After incubation, the liposomes were stored at 4 °C until needed for experiments.

D. DIC Microscopy

For microscopy experiments, tau tagged with Alexa Fluor-546 (excitation/emission: 561nm/572nm) was thawed over ice and solutions of 0.73 $\mu\text{g}/\mu\text{L}$ tau (1.59×10^{-14} M) in varying salt solutions (0-300mM) were created in separate Eppendorf tubes at room temperature. 3 μL of each solution was placed on microscope slides, along with a coverslip and parafilm to maintain a seal. The samples were immediately imaged on the Nikon Eclipse Ti2 Microscope at 20x, 40x, or 60x objective with the addition of a 1.5x lens.

Liposomes are retrieved from 4°C and mixed into varying salt concentrations (10-300mM) in separate Eppendorf tubes at room temperature. Molar compositions of liposomes varied based on the experimental objective. Microscope slides were created and samples were imaged in the same format as aforementioned.

Liposome samples prepared at 60μM concentration were mixed with 0.73 μg/μL tau (1.59x10⁻¹⁴ M) at a volume charge density (ρ) of 1 in an Eppendorf tube in varying salt solutions (0-300mM). Similarly, two different types of tau tagged with fluorophores were used depending on the liposome mixture. If liposomes were tagged with a fluorophore (Cy5.5 PE lipid - excitation/emission 683nm/703nm), then tau tagged with Alexa-488 (Alexa 488 excitation/emission: 488nm/496nm) was used whereas Alexa-546 (Alexa 546 excitation/emission: 561nm/572nm) tau was used when lipids were not labeled. The sample solutions of the liposome-tau mixture were stored at room temperature for the duration of the experiment. The microscope slide containing the liposome-tau mixture was created and imaged using the previous protocol for imaging tau alone.

E. Fluorescence Microscopy

Microscope slides were prepared using the same method outlined for DIC and imaged with the Nikon Eclipse Ti2 in fluorescence mode. To observe the liposomes present in the sample, the Cy5 (Cyanine 5) filter was used (Cy5.5 PE lipid - excitation/emission 683nm/703nm). To observe tau present, either the GFP (Green fluorescent protein) channel (Alexa Fluor 488; excitation/emission: 488nm/496nm) or the RFP (Red fluorescent protein) channel was used (Alexa Fluor 546; excitation/emission: 561nm/572nm). Again, the samples were viewed using the 20x, 40x, or 60x objective with the addition of a 1.5x lens.

III. Results and Discussion

A. Salt-Dependent Behavior of 4RL Tau Self-Coacervates

In an aqueous system with very low ionic strength, 4RL tau made up of 441 amino acids is found to form stable liquid-liquid phase separated (LLPS) droplets due to self-coacervation of tau molecules depicted in the cartoon in figure 2a. Figure 2 (b-f) shows differential-interference-contrast (DIC) micrographs of tau self-coacervates as a function of increasing ionic strength between 0 mM and 300 mM KCl. Here, we used full length 4RL-tau tagged with Alexa-546, in order to carry out near simultaneous DIC and fluorescence experiments on the same samples. At 0mM (deionized Milli-Q; pH 6.998) and 10 mM KCl, there is an abundance of tau droplets as shown in figure 2 (Fig. 2b, 2c and zoomed-in section shown in “l”). The observation of stable droplets is due to protein tau’s inherent polyampholyte nature leading to self-coacervation with intermolecular electrostatic interactions, between and within tau chains (Fig. 2a). To form tau self-coacervates, the cationic sections of 4RL-tau (Fig. 1a), made up of the PRR (amino acid 152-240) and the MTBR (amino acid 241-368) domains containing exon 10 and thus all 4 repeats, must have favorable electrostatic interactions with the anionic domains, at the N- and C- terminals made up of the PD (amino acid 1-151) containing the inclusion of exon 2 and 3 and the CTT (amino acid 369-441).

A significant contrasting behavior is observed with increasing salt concentration where at 50mM KCl (Fig. 2d and zoomed-in section shown in “m”), there are far fewer particles and almost little to none at 150mM KCl near physiological (1:1 electrolyte) salt concentrations with Debye screening length $\lambda_D \approx 0.785$ nm (Fig. 2e and zoomed-in section shown in “n”). Thus, there is a clear decrease in particle concentration with increasing ionic strength between

10 mM and 150 mM. The observation of dissolution of tau self-coacervate droplets implies a significant decrease in the attractive electrostatic forces between anionic and cationic domains of tau due to enhanced charge screening and decreased Debye screening length from $\lambda_D \approx 3.04$ nm to ≈ 0.962 nm.

The breakdown of tau self-coacervates is more clearly seen in fluorescence images of the same particles (with 4RL-tau tagged with Alexa-546 visible in the RFP channel) previously observed in DIC (Fig. 2g-k). At 0mM and 10mM KCl (Fig. 2g, 2h) there is again an abundance of particles and little diffuse background indicative of free tau. Alternatively, at 50mM (Fig. 2i), there are far fewer particles and the background fluorescence is increasing, showing a coexistence of tau coacervates and tau dispersed in solution. At 150mM KCl (Fig. 2j), near physiological salt concentrations (1:1 electrolyte), there are almost no particles and the background is mostly diffused, showing that the majority of tau is no longer in the LLPS droplet state. However, on occasion a small amount of coacervates are observed in the high salt regimes as indicated by the white circle in Fig. 2j. This observation is consistent with previous studies at high salt where it was found that the tau self-coacervates can retain their stability only with the addition of a depletant such as poly-(ethylene-oxide) (PEO), giving rise to PEO-induced depletion attraction between tau chains, phase separation and droplet formation.^{36,37}

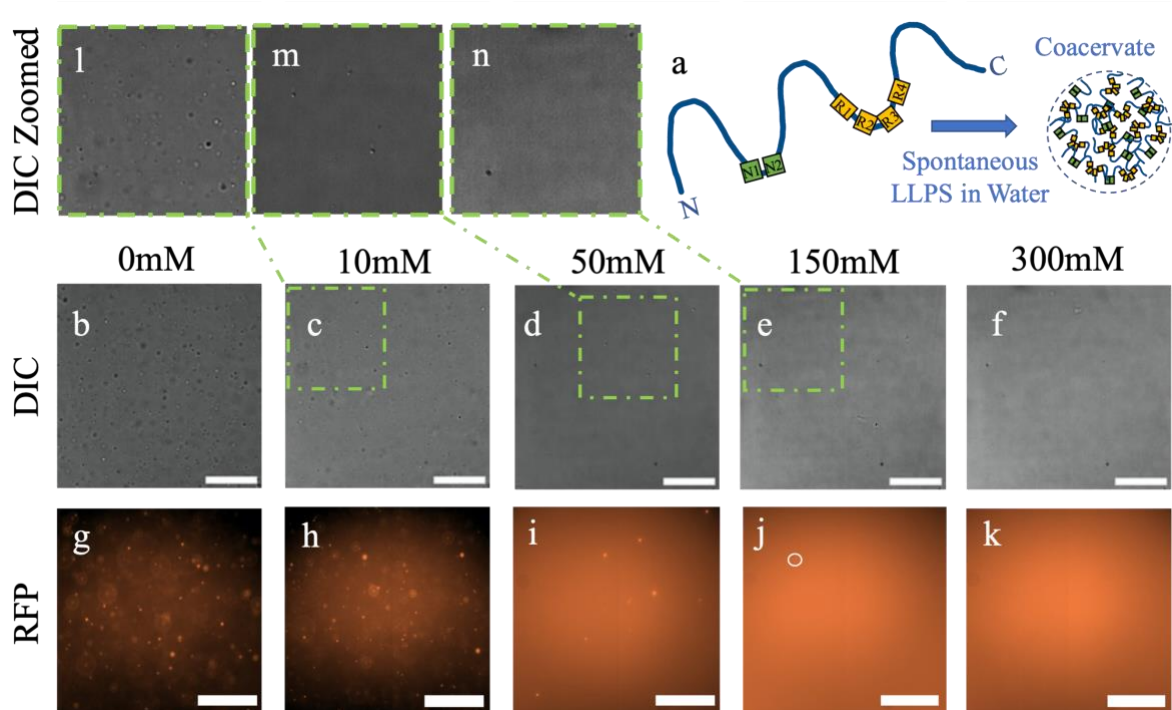


Figure 2. Electrostic interactions of tau coacervates break near physiological salt concentration. (a) Cartoon of 4RL undergoing intermolecular electrostatic interactions to create a tau coacervate in deionized water. (b-f) Differential interference contrast (DIC) microscopy images of full length 4RL tau tagged with Alexa-546 in increasing KCl concentrations (0-300mM). (g-k) Fluorescent microscopy of full length 4RL tau tagged with Alexa-546 visible in the RFP channel (Alexa 546 excitation/emission: 561nm/572nm) in increasing KCl concentrations (0-300mM). (l-n) Zoomed-in inset of corresponding DIC images linked by dashed line scaled by a factor of 2. All scale bars = 50 μ m.

B. Anionic Liposomes at Low and High Salt Concentrations

Figure 3a depicts the chemical structures of the lipid components used when forming the anionic liposomes: DOPS (charge = -1e), DOPG (charge = -1e), DOPC (C18:1, zwitterion, charge = 0) and a small amount of Cy5.5-PE (C18:1) to add a fluorescent tag. Due to lipids poor solubility in water, they are mixed in an organic solvent, allowing each individual lipid component to easily dissolve. This creates liposomes made up of a uniform mixture. The anionic liposomes had a composition of either (50% DOPG/ 49%DOPC/1% CY5.5 PE) or (50% DOPS/ 49%DOPC/1% CY5.5 PE).

Figure 3 (b-d) shows DIC of anionic liposomes as a function of increasing ionic strength between 10 mM and 300 mM KCl. The number of liposomes remain nearly constant between 10mM (Fig. 3b) and 300mM (Fig. 3d), suggesting that the anionic liposomes are stable and retain their structure under both low and high ionic strengths. This can be seen more clearly in the corresponding zoomed in insets (Fig. h-j). This is further confirmed in fluorescence images of the same particles previously observed in DIC (Fig. 2e-g). Both the background and the concentration of particles appear similar between 10mM KCl (Fig. 3e) to 300mM KCl (Fig. 3g).

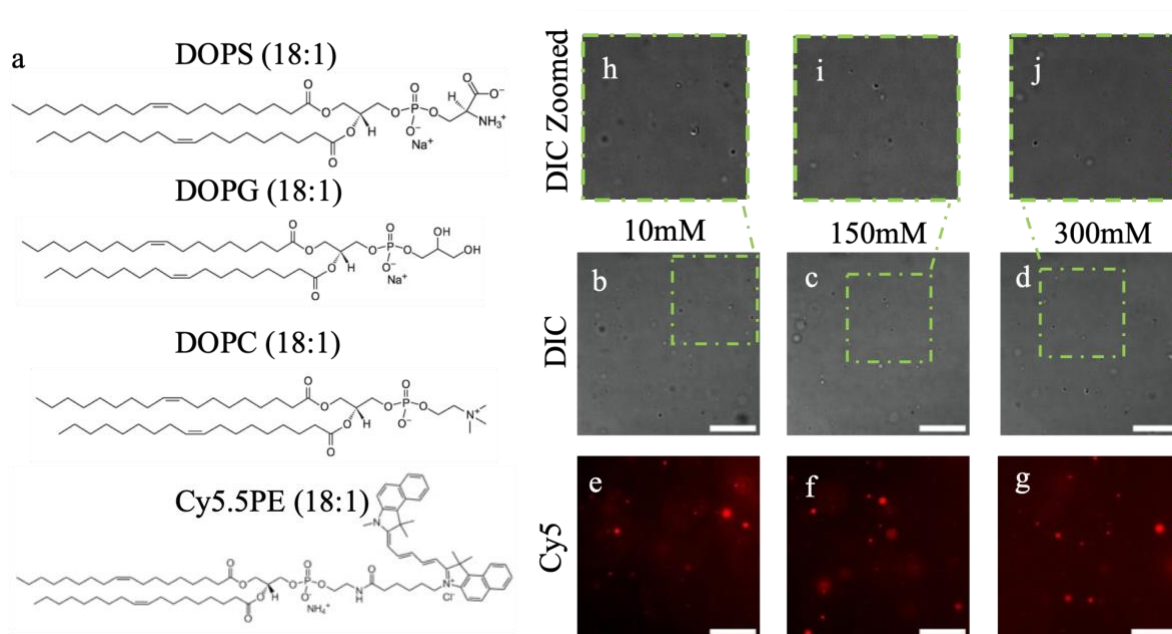


Figure 3. Observation of anionic liposomes at low and high salt conditions. (a) Chemical structures of DOPS (C18:1, Q =-1), DOPG (C18:1, Q =-1), DOPC (C18:1, zwitterion) and Cy5.5-PE (C18:1) lipids used to make anionic liposomes for experiments.⁴² (b-d) DIC microscopy images of unsonicated anionic liposomes tagged with Cy5.5-PE (50% DOPS/49%DOPC/1% CY5.5 PE) in increasing KCl concentrations (10-300mM). (e-g) Fluorescent microscopy of unsonicated anionic liposomes tagged with Cy5.5-PE (50% DOPS/49%DOPC/1% CY5.5 PE) visible in the Cy5 channel (Cy5.5 PE lipid - excitation/emission 683nm/703nm) in increasing KCl concentrations (10-300mM). (h-j) Zoomed-in inset of corresponding DIC images linked by dashed line scaled by a factor of 2. All scale bars = 50µm.

C. Phase Separated States in Mixtures of Anionic Liposomes and Tau in Deionized Water

To elucidate the types of distinct states/structures that are formed when anionic liposomes (ALs) interact with polyampholyte tau in the regime where electrostatic interactions are the strongest, we studied a reaction mixture of tau and liposomes in deionized water containing either DOPS (-1) or DOPG (-1). Phosphatidylserine (PS) based anionic lipids are among the primary lipids imparting negative charge to mammalian plasma membranes, whereas, lipids with phosphatidylglycerol (PG) headgroups constitute a second class of anionic lipids occurring at a lower content (1-2%) compared to PS-based anionic lipids.¹² Figure 4 (a) shows optical fluorescent images of ALs (50% DOPG/ 49%DOPC and 1% CY5.5-PE fluorescent in the CY5 (red) channel mixed in deionized water with 4RL-tau tagged with Alexa-488, fluorescent in the GFP (green) channel, at a lipid/tau molar charge ratio, $\rho=1$. A z-stack of images in the x-y plane (with merged GFP and CY5 channels), allows for visualization of the 3D structures of the particles in the x-y, y-z, and x-z planes and reveals three distinct phase separated states.

Particles labeled 1 and 2 in figure 4a, visible in both GFP and CY5 channels, are characterized as anionic liposome-tau complexes. In the first AL-tau complex state (labeled “1” in figure 4a with expanded views in the top four panels in figure 4b), 4RL-tau (seen in the GFP channel) coats the perimeter of a giant multilamellar liposome. Furthermore, smaller liposomes with bound tau and attached to the giant liposome may also be seen with the smaller vesicles in the Cy5 channel and the corresponding tau clumps in the GFP channel. The green (tau) and red (lipid) intensity scans through the AL-tau complex (Figure 4b, lower panel), are consistent with the described structure where you can see the overall “U” shape and the asymmetric distribution of tau (green line) around the giant multilamellar vesicle (red line).

A second distinct AL-tau complex state observed (labeled “2” in figure 4a with expanded views in the top four panels in figure 4c), consists of an assembly of small liposomes glued together through the cationic domains of 4RL-tau bound to the surface of the vesicles. This is confirmed in the particle images where individual spheres bundled together are observed in the GFP, the CY5, and the GFP/CY5 merged channels. The green (tau) and red (lipid) intensity profiles in figure 4c show multiple peaks for both GFP and Cy5 channels consistent with an assembly of tau-coated vesicles. The morphology of the tau-mediated assembly of small liposomes is similar to that of vesosomes used in drug delivery applications where in that system the small neutral vesicles are brought together from confinement forces within a membrane bilayer.^{36,41,42}

A third distinct phase separated state further appears in mixtures of ALs and tau. This particle labeled “3” in figure 4a (with expanded views in the top four panels in figure 4d) is an example of self-coacervation of polyampholyte tau through intermolecular electrostatic interactions between the anionic and cationic domains (figure 1 and 2a). As expected for a liquid-liquid phase separated state, the particle, which is seen in the GFP channel but not the CY5, is spherical. Consistently, the green (tau) and red (lipid) intensity profiles in figure 4d display a highly symmetrical tau peak indicative of a liquid coacervate with no evidence of any lipid assembly.

Figure 5 displays fluorescent images similar to those of figure 4, but instead examines the interaction of 4RL-tau (tagged with Alexa-488) and anionic liposomes with composition (50% DOPS/ 49%DOPC/1% CY5.5 PE) in deionized water, where DOPG is replaced by DOPS at a lipid/tau charge ratio, $\rho=1$. Three particles with different structures are identified in Figure 5a displaying images in the x-y, x-z, and y-z planes with the GFP and CY5 channels merged.

The expanded images of particle 1 (top panels (CY5, GFP, GFP/CY5, DIC) in figure 5b) display another example of 4RL-tau decorating the perimeter of a GUV with the same “U” shape green and red intensity profiles (figure 5b). For this particle, fewer small liposome-tau complexes are observed to be attached to the giant multilamellar liposome, compared to particle 1 from figure 4. Particle 2 is another example of an assembly of small liposomes fused together by tau.

In contrast, particle 3 (top panels (CY5, GFP, GFP/CY5, DIC) in figure 5d) displays a less commonly observed structure in mixtures of ALs and tau. A tau coacervate (dense semi-spherical particle in the top right in the GFP-tau channel) adsorbed on a non-spherical AL-tau complex consisting of one or more tau-coated liposomes visible in the GFP channel with hollow regions typical of liposomes. The GFP (tau) intensity profile (lower panel, figure 5d), which displays multiple peaks is supportive of a tau-coacervate interacting with an AL-tau complex. In contrast to the strong GFP intensity profile, there is mainly a small visible shape in the Cy5 channel that is not picked up in the red intensity profile (figure 5d). Intensity profiles taken in the x-y plane through different sections of the nonspherical shaped particle (with a concave distortion) in the Cy5 channel are similarly flat (Appendix, figure 1). This is consistent with the nonspherical liposome being unilamellar with relatively few fluorescent lipids sampled in the line scans.

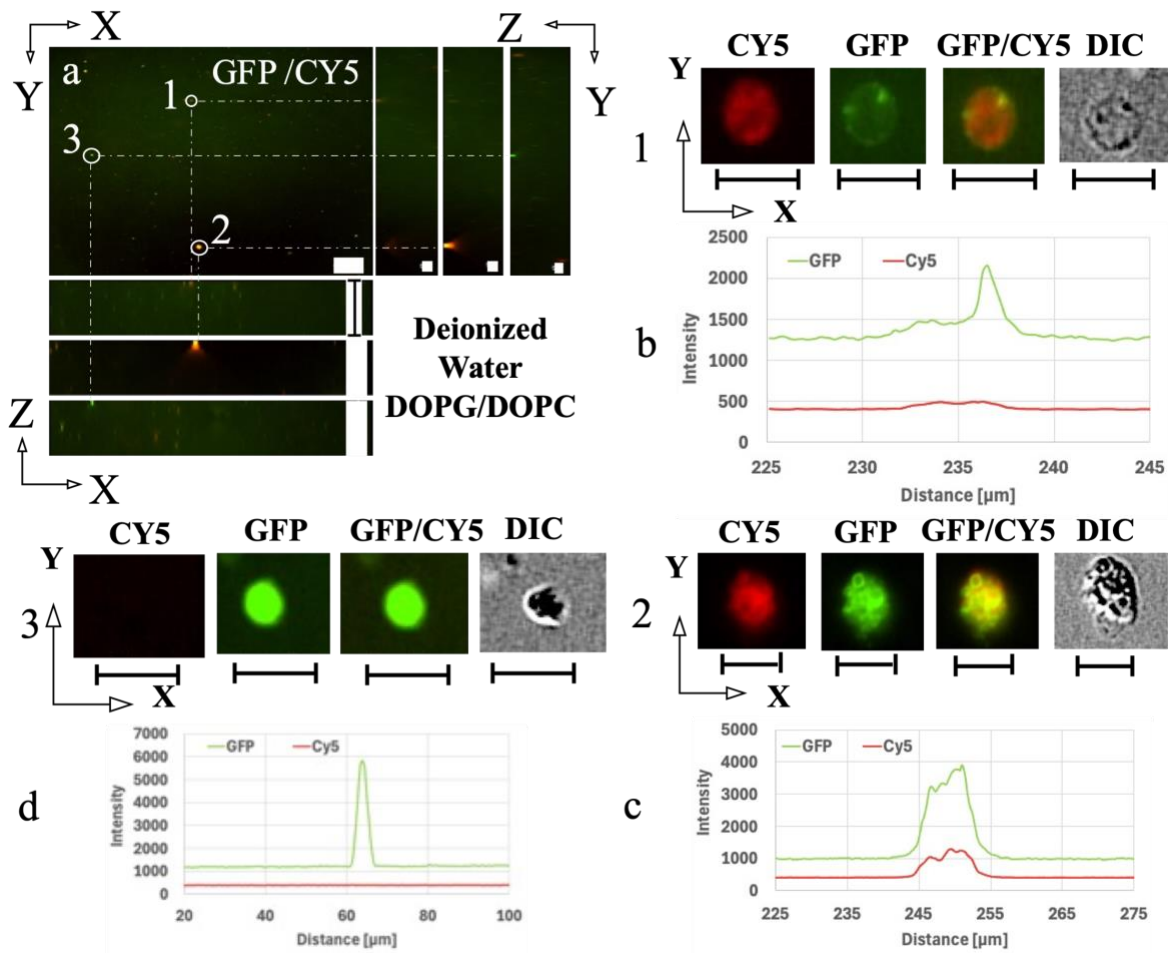


Figure 4. Fluorescent microscopy images of anionic liposomes made of 50% DOPG/49%DOPC/1% CY5.5 PE interacting with 4RL tau in deionized water. The lipid channel (Cy5) is shown in RED (excitation/emission 683nm/703nm) and 4RL tau tagged with Alexa-488, is shown in the GFP channel (GREEN) (excitation/emission: 488nm/496nm). (a) A 3D Z-stack image series showing both GFP and Cy5 channels. The main image frame (top left panel) shows the X-Y section view at a chosen Z. The projection to the right shows the Y-Z side views slicing along the vertical dotted lines of three circled objects. The bottom panel shows the X-Z slices along the horizontal dotted lines. The X-Z and Y-Z plane side views of each circled object are indicated by the end of the dotted lines in each direction. (Scale bars correspond to 50μm in the X-Y plane, 200μm in X-Z and 20μm in Y-Z planes, respectively) (b) Detail view of particle 1: a giant liposome-4RL tau complex. Top panel from left to right: magnified fluorescent (Cy5, GFP and GFP/Cy5 overlay) and DIC images of particle 1. Bottom panel: fluorescent intensity profiles of particle 1 in Cy5/GFP channels as a function of X. (c) Detail view of particle 2: an anionic liposome-4RL tau complex shown in magnified fluorescent (Cy5, GFP and GFP/Cy5 overlay) and DIC images, and fluorescent intensity traces as a function of X. (d) Detail view of particle 3: a tau coacervate with lipid assembly shown in magnified fluorescent (Cy5, GFP and GFP/Cy5 overlay) and DIC images, and fluorescent intensity traces as a function of X. Scales bar in (b-d) = 10μm.

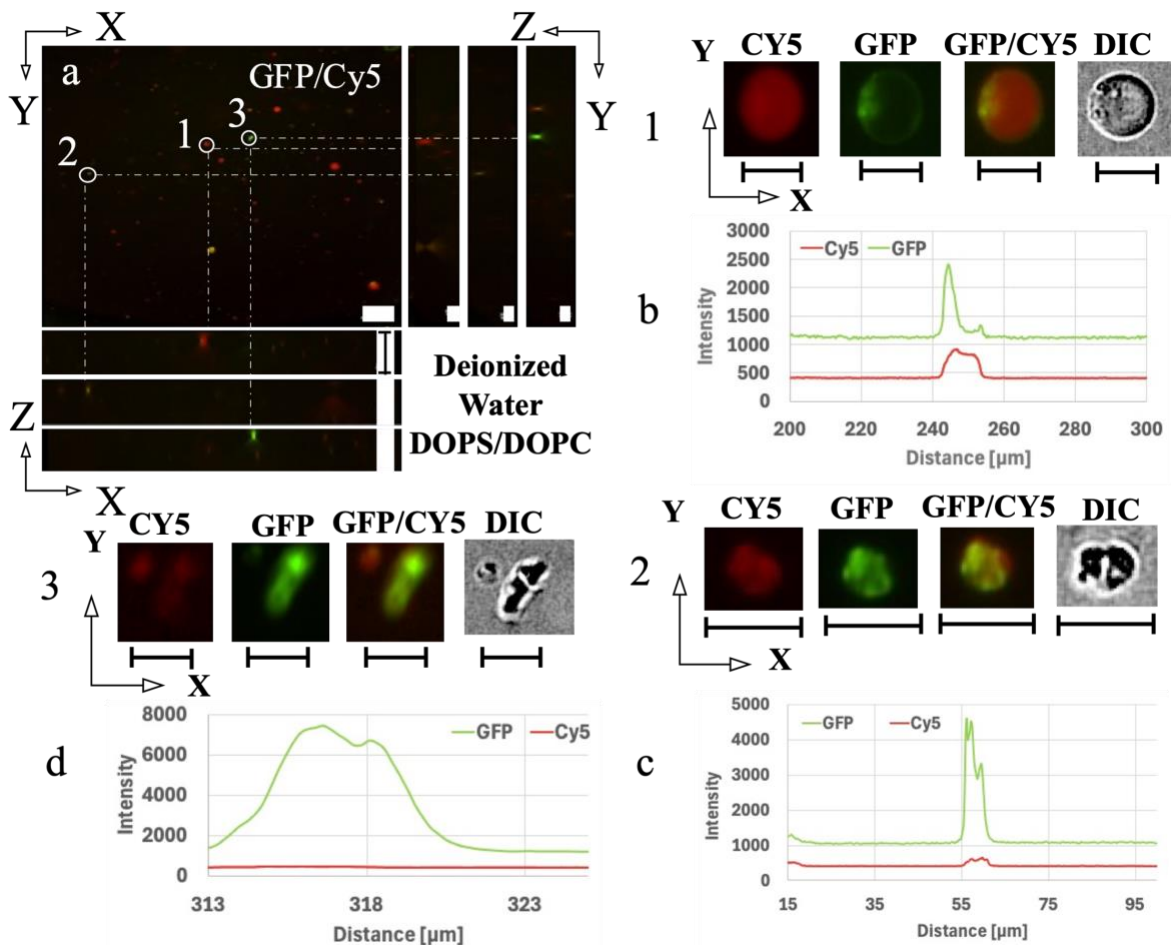


Figure 5. Fluorescent microscopy images of anionic liposomes made of 50% DOPS/49% DOPC/1% CY5.5 PE and 4RL tau in deionized water. The lipid channel is shown in the RED Cy5 channel (excitation/emission 683nm/703nm) and 4RL tau tagged with Alexa-488 is shown in GREEN in the GFP channel (excitation/emission: 488nm/496nm). (a) A Z-stack image series showing both GFP and Cy5 channels. The top left frame shows the X-Y plane view at a chosen Z. The three panels to the right show the Y-Z slices along vertical dotted lines marking three circles objects 1-3. The bottom panels are the X-Z side views (slices) along the horizontal dotted lines of circles objects 1-3. The Z-X and Y-Z plane side views of each circled object are indicated by the end of the dotted lines in each direction. (Scale bars correspond to 50 μ m in the X-Y, 200 μ m in X-Z and 20 μ m in Y-Z planes, respectively) (b) Detail view of particle 1: a giant liposome-4RL tau complex. Top panel from left to right: magnified fluorescent (Cy5, GFP and GFP/Cy5 overlay) and DIC images of particle 1. Bottom panel: fluorescent intensity profiles of particle 1 in Cy5/GFP channels as a function of X. (c) Detail view of particle 2: an anionic liposome-4RL tau complex shown in magnified fluorescent (Cy5, GFP and GFP/Cy5 overlay) and DIC images, and fluorescent intensity traces as a function of X. (d) Detail view of particle 3: a tau coacervate with lipid assembly shown in magnified fluorescent (Cy5, GFP and GFP/Cy5 overlay) and DIC images, and fluorescent intensity traces as a function of X. Scales bar in (b-d) = 10 μ m.

D. Comparison of Phase Separated States in Mixtures of Anionic Liposomes and Tau in Low versus High Salt

Figure 6 compares mixtures of unlabeled anionic liposomes (50% DOPG/ 50% DOPC) and 4RL-tau tagged with Alexa-546, fluorescent in the RFP channel, at low and high salt concentrations in DIC and the corresponding fluorescent images. Two different salts, KCl and NaCl were used to mimic physiological 1:1 electrolytes. Figures 6a, 6c, 6e, and 6g show the interactions at a low ionic strength of 5mM, while figures 6b, 6d, 6f, and 6h were performed at a high ionic strength 150mM and the particles detected in the RFP channel were circled. There is a clear decrease in the number of particles in the DIC micrographs as the mixture transitioned from low (5 mM, fig. 6a, 6e) to high salt (150 mM, fig. 6b, 6f). Remarkably, the corresponding fluorescence images show that the decrease in particle density is accompanied by an increase in background fluorescence due to free labeled tau as the mixtures transition from low (fig. 6c, 6g) to high salt (fig. 6d, 6h).

At the low ionic strengths, the particles observed in DIC and fluorescence micrographs from labeled tau (fig. 6a, 6c, 6e, and 6g) include both tau coacervates and AL-tau complexes. For tau alone preparations at increasing salt concentrations, we observed that tau self-coacervates dissolved at concentrations between 100 mM and 150 mM (with very few coacervates remaining at 150 mM) leading to the observed increase in fluorescence background due to free tau. Thus, the observed particles at 150 mM NaCl or KCl (fig. 6b, 6d, 6f, and 6h), mainly correspond to AL-tau complexes, which remain stable while coacervate droplets disperse into free tau.

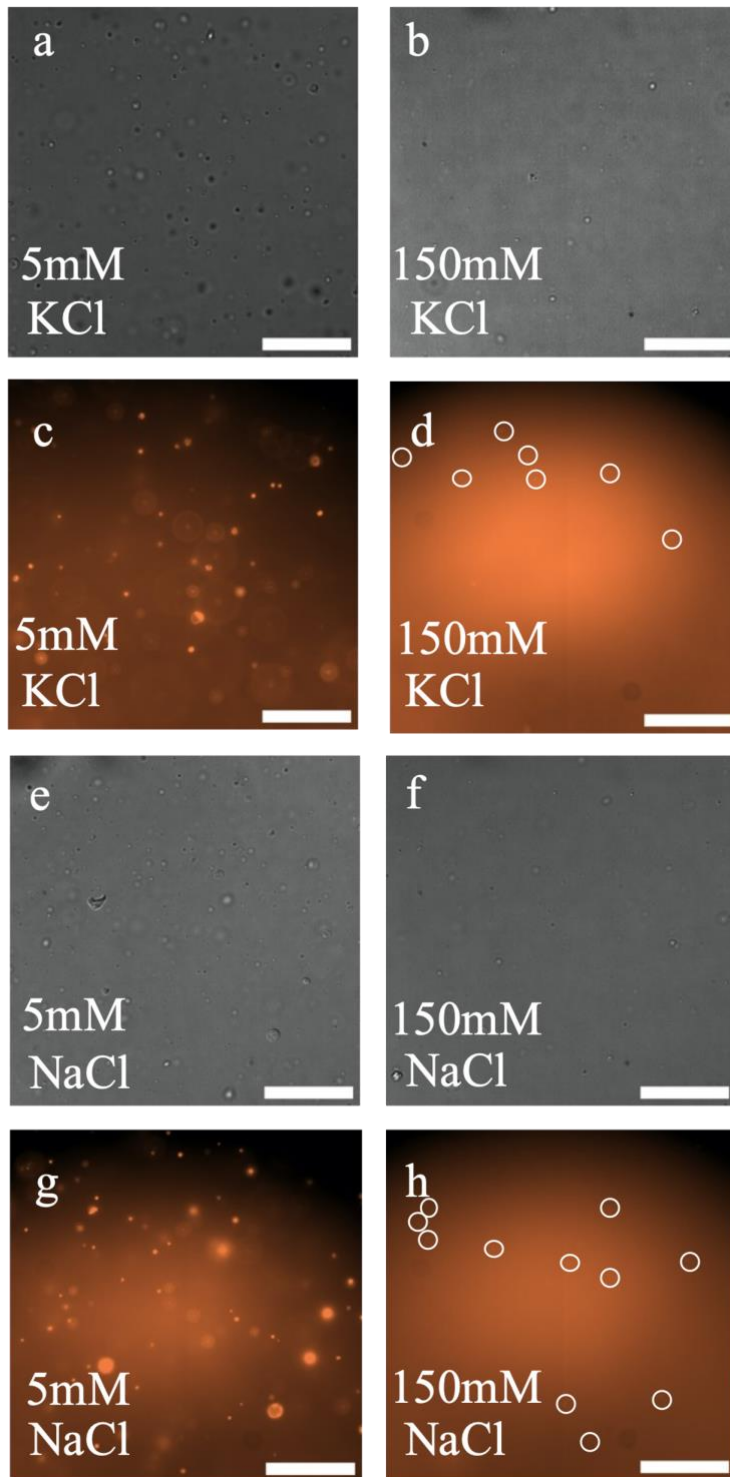


Figure 6. Electrostatic interactions in tau coacervates are weaker than anionic liposome-tau interactions. (a, b) DIC microscopy images of full length 4RL tau tagged with Alexa-546 and unlabeled anionic lipids (50 mol% DOPG/ 50 mol% DOPC) in low (5mM) and high (150mM) KCl concentrations. (c, d) fluorescent microscopy images in the RFP channel corresponding to (a,b) showing full length 4RL tau tagged with Alexa-546 (excitation/emission: 561nm/572nm). [50 μ m scale bar] (e, f) DIC microscopy images of full length 4RL tau tagged with Alexa-546 and unlabeled anionic lipids (50 mol% DOPG/ 50 mol% DOPC) in low (5mM) and high (150mM) NaCl concentrations. (g, h) RFP fluorescent images corresponding to DIC images shown in (e, f). [50 μ m scale bar]

E. Mixture of Anionic Liposomes and Tau in Low Salt

Figure 7, 8, and 9 display the interactions of 4RL tau and anionic liposomes (50% DOPS/ 49% DOPC/1% CY5.5 PE) in a solution of low ionic strength. The same methods were used as in figures 4 and 5, but instead of deionized water, the two were mixed in a solution of 10mM KCl. The z-stack of this mixture showed the persistence of the three phase states; however, it is clear the background is already starting to increase due to some of the dissolution of the tau self-coacervate. Figures 7, 8, and 9 correspond to the three different states respectively, each examining a different z-plane of the same mixture. Figure 7 shows the different cuts of particle 1, another giant liposome/tau complex with one nominal GUV and other liposomes glued on by tau. Figure 8 visualizes particle 2, an example of 4RL tau coating the surface of the outer lipid membrane. In this case again, it is likely this is multiple liposome-tau complexes fused together as seen through the numerous peaks on its corresponding intensity map, figure 8b. Last particle 3 in figure 9 is again a symmetric spherical object illuminated solely in the GFP channel indicating that this is likely a tau coacervate with no lipid assembly.

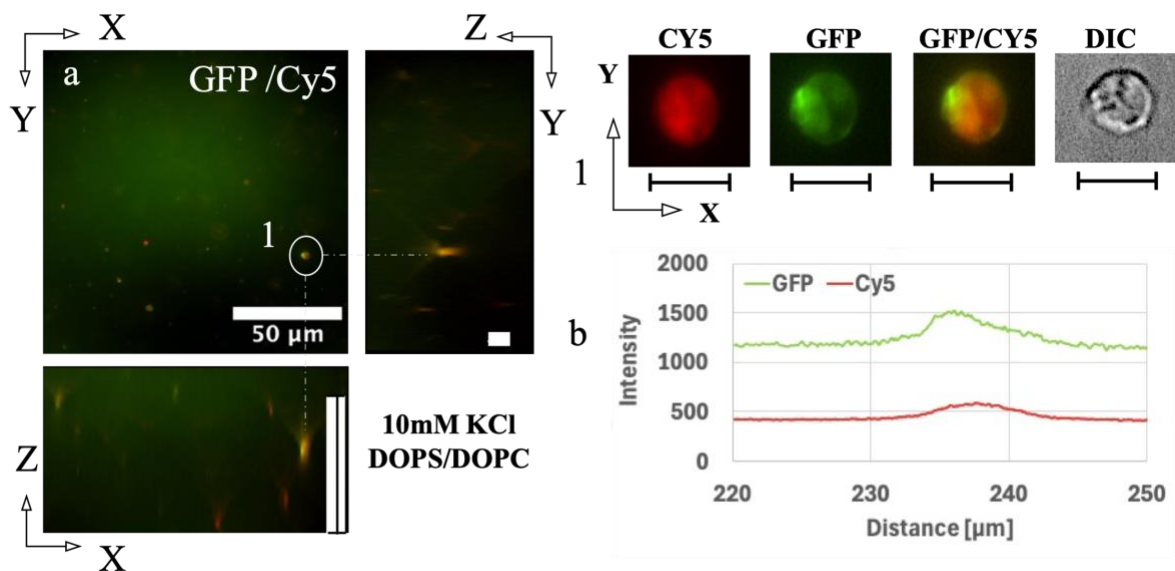


Figure 7. Fluorescent microscopy images of anionic liposomes and 4RL tau in 10mM KCl. The anionic liposomes made from 50% DOPS/ 49%DOPC/1% CY5.5 PE are visible in the Cy5 channel (RED) (Cy5.5 PE lipid - excitation/emission 683nm/703nm) and 4RL tau tagged with Alexa-488 (Alexa 488 excitation/emission: 488nm/496nm) are visible in the GFP channel (green). (a) A Z-stack image showing both GFP and Cy5 channels. The top left frame shows the X-Y section view at a chosen Z. The panels to the right show the Y-Z slice along the vertical dotted line marking the circled object 1. The bottom panel shows the X-Z section along the horizontal dotted line of object 1. (Scale bars correspond to 50 μ m in the X-Y, 200 μ m in X-Z and 20 μ m in Y-Z planes, respectively) (b) Detail view of particle 1: a giant anionic liposome-4RL tau complex. Top panel from left to right: magnified fluorescent (Cy5, GFP and GFP/Cy5 overlay) and DIC images of particle 1. Bottom panel: fluorescent intensity profiles of particle 1 in Cy5/GFP channels as a function of X. [*10 μ m scale bars*]

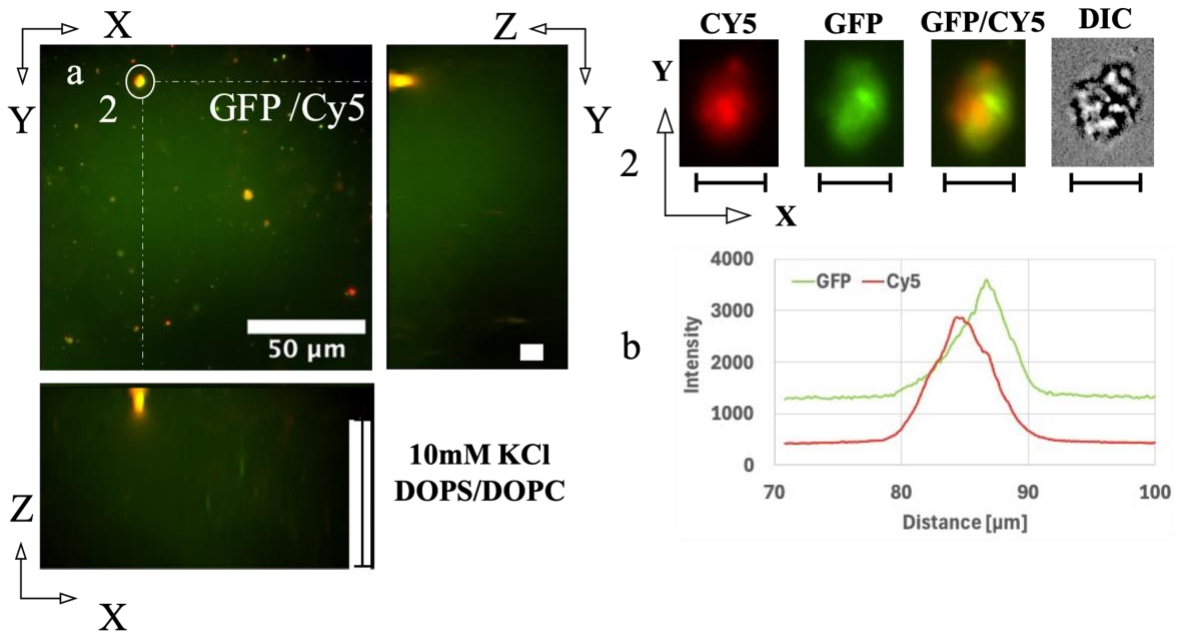


Figure 8. Fluorescent microscopy images of anionic liposomes and 4RL tau in 10mM KCl. The anionic liposomes made from 50% DOPS/ 49%DOPC/1% CY5.5 PE are visible in the Cy5 channel (RED) (Cy5.5 PE lipid - excitation/emission 683nm/703nm) and 4RL tau tagged with Alexa-488 (Alexa 488 excitation/emission: 488nm/496nm) are visible in the GFP channel (green). (a) A Z-stack image showing both GFP and Cy5 channels. The top left frame shows the X-Y section view at a chosen Z. The panels to the right show the Y-Z slice along the vertical dotted line marking the circled object 2. The bottom panel shows the X-Z section along the horizontal dotted line of object 2. (Scale bars correspond to 50 μ m in the X-Y, 200 μ m in X-Z and 20 μ m in Y-Z planes, respectively) (b) Detail view of particle 2: a anionic liposome-4RL tau complex. Top panel from left to right: magnified fluorescent (Cy5, GFP and GFP/Cy5 overlay) and DIC images of particle 2. Bottom panel: fluorescent intensity profiles of particle 2 in Cy5/GFP channels as a function of X. [*10 μ m scale bars*]

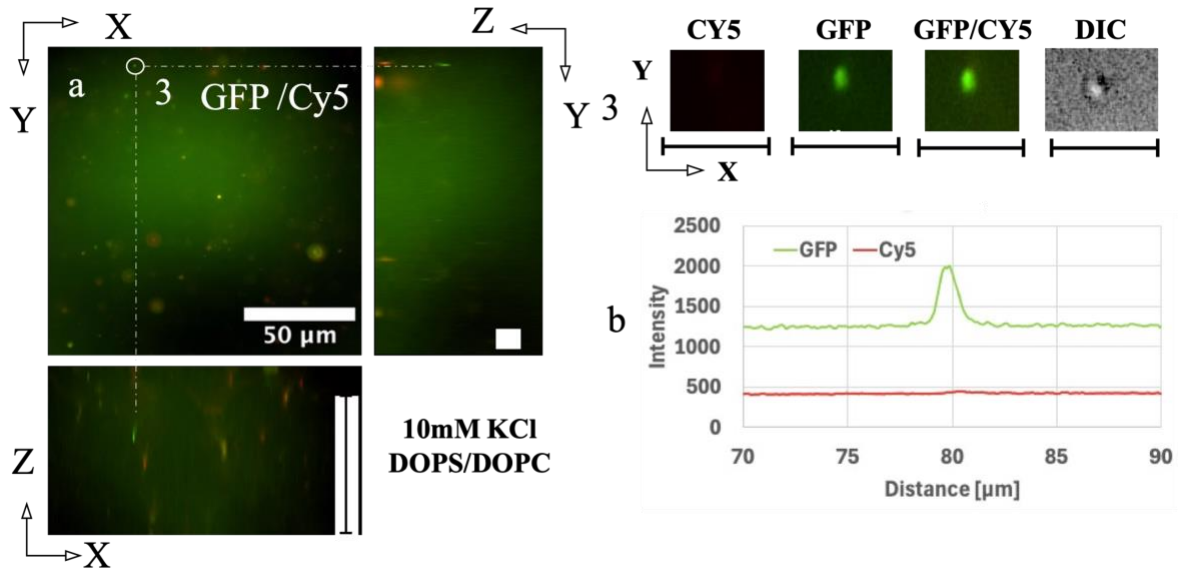


Figure 9. Fluorescent microscopy images of anionic liposomes and 4RL tau in 10mM KCl. The anionic liposomes made from 50% DOPS/ 49%DOPC/1% CY5.5 PE are visible in the Cy5 channel (RED) (Cy5.5 PE lipid - excitation/emission 683nm/703nm) and 4RL tau tagged with Alexa-488 (Alexa 488 excitation/emission: 488nm/496nm) are visible in the GFP channel (green). (a) A Z-stack image showing both GFP and Cy5 channels. The top left frame shows the X-Y section view at a chosen Z. The panels to the right show the Y-Z slice along the vertical dotted line marking the circled object 3. The bottom panel shows the X-Z section along the horizontal dotted line of object 3. (Scale bars correspond to 50μm in the X-Y, 200μm in X-Z and 20μm in Y-Z planes, respectively) (b) Detail view of particle 3: a tau coacervate. Top panel from left to right: magnified fluorescent (Cy5, GFP and GFP/Cy5 overlay) and DIC images of particle 3. Bottom panel: fluorescent intensity profiles of particle 3 in Cy5/GFP channels as a function of X. [*10μm scale bars*]

F. Mixture of Anionic Liposomes and Tau in High Salt

Consistent with the data shown in figure 6 mostly lacking tau self-coacervates in the high salt regime, another less common but noteworthy structure, observed in mixtures of ALs (50% DOPS/ 49%DOPC/1% CY5.5 PE) and tau in 100 mM KCl, consisted of AL-tau complexes displaying an assembly of tau-free “bare” liposomes trapped inside a giant multilamellar vesicle (i.e. similar to vesosomes [34]) but now with tau decorating the outside perimeter. This is shown in figure 10 (labeled “1” in the merged GFP and CY5 channels in figure 10a with expanded views in the top four (CY5, GFP, GFP/CY5, DIC) panels in figure 10b). The lack of tau associated with the internal vesicles can be seen in comparing the GFP (tau) and CY5 (lipid) channels, where tau coats the giant liposome surface and also a few much smaller bound liposomes. The GFP (tau) and red (lipid) intensity profiles (lower panel, figure 10b) are also consistent with the observed structures in the x-y plane in the GFP, CY5, and GFP/CY5 channels. Figure 11 shows particle 2, another liposome-tau complex where 4RL tau coats the surface of the outer lipid membrane. No coacervates (which are rare at these salt concentrations) were found in this mixture at 100 mM and the background GFP fluorescence indicative of dispersed tau is significantly higher compared to mixtures at 10 mM KCl. It is likely that in the high ionic solution, the electrostatic interactions of the LLPS state break causing the tau to dissolve into the background and little to no coacervates to remain. It should also be noted that at this high salt, no tau-free liposomes remain, instead they only exist as AL-tau complexes.

In figures 12, 13, and 14, the salt concentration is increased to 150mM, physiological conditions (1:1) and again, the background of the mixture was increased due to the increase in diffused tau. Figures 12, 13, and 14 correspond to the three different states respectively,

each examining a different z-plane of the same mixture. In this mixture the first particle identified is another case in which tau coats the perimeter of the giant liposome. This can be confirmed by the shape of the intensity profile, figure 12b. Figure 13 visualizes particle 2, an example of 4RL tau coagulating along the surface of the outer lipid membrane. Potentially, this is a complex built of many small liposomes connected by tau. Last a rare sighting of a tau coacervate with some lipid assembly was found and labeled as particle 3 in figure 14. This is likely not a true coacervate due to the shape of the particle. After numerous attempts to find a true coacervate were conducted, it was clear that even finding this particle was rare due to the high ionic strength of the solution.

Taken together, our observation indicates that the electrostatic interactions between the cationic domains of tau and anionic membranes are significantly stronger than the electrostatic interactions stabilizing tau self-coacervates and tau self-coacervate droplets are found to dissolve with dispersed tau with increasing (1:1) salt concentrations.

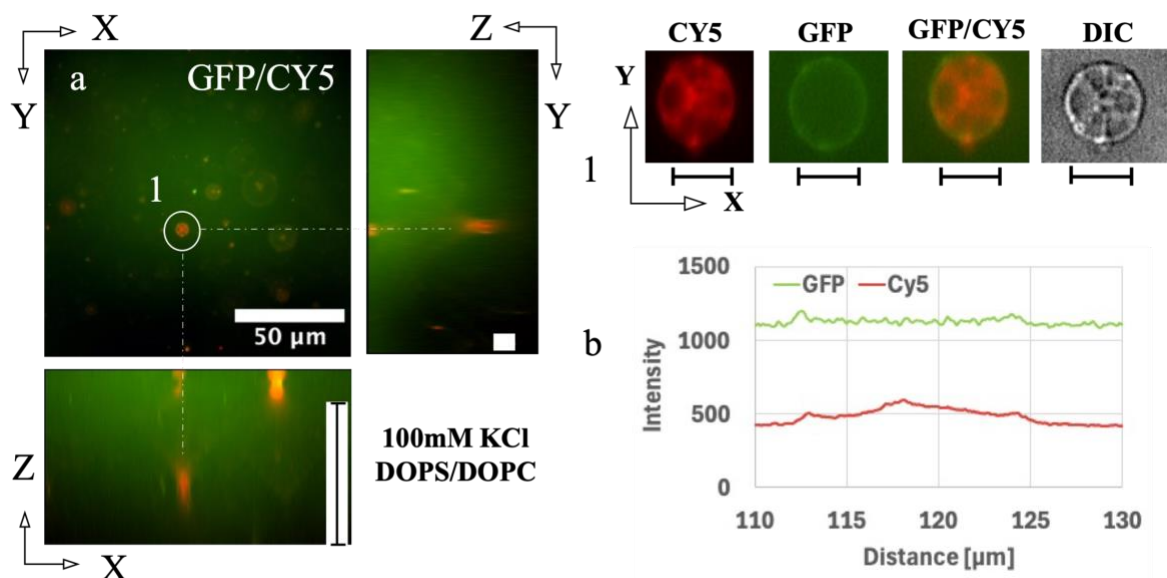


Figure 10. Fluorescent microscopy images of anionic liposomes and 4RL tau in 100mM KCl. The anionic liposomes made from 50% DOPS/ 49%DOPC/1% CY5.5 PE are visible in the Cy5 channel (RED) (Cy5.5 PE lipid - excitation/emission 683nm/703nm) and 4RL tau

tagged with Alexa-488 (Alexa 488 excitation/emission: 488nm/496nm) are visible in the GFP channel (green). (a) A Z-stack image showing both GFP and Cy5 channels. The top left frame shows the X-Y section view at a chosen Z. The panels to the right show the Y-Z slice along the vertical dotted line marking the circled object 1. The bottom panel shows the X-Z section along the horizontal dotted line of object 1. (Scale bars correspond to 50 μ m in the X-Y, 200 μ m in X-Z and 20 μ m in Y-Z planes, respectively) (b) Detail view of particle 1: a giant anionic liposome-4RL tau complex. Top panel from left to right: magnified fluorescent (Cy5, GFP and GFP/Cy5 overlay) and DIC images of particle 1. Bottom panel: fluorescent intensity profiles of particle 1 in Cy5/GFP channels as a function of X. [*10 μ m scale bars*]

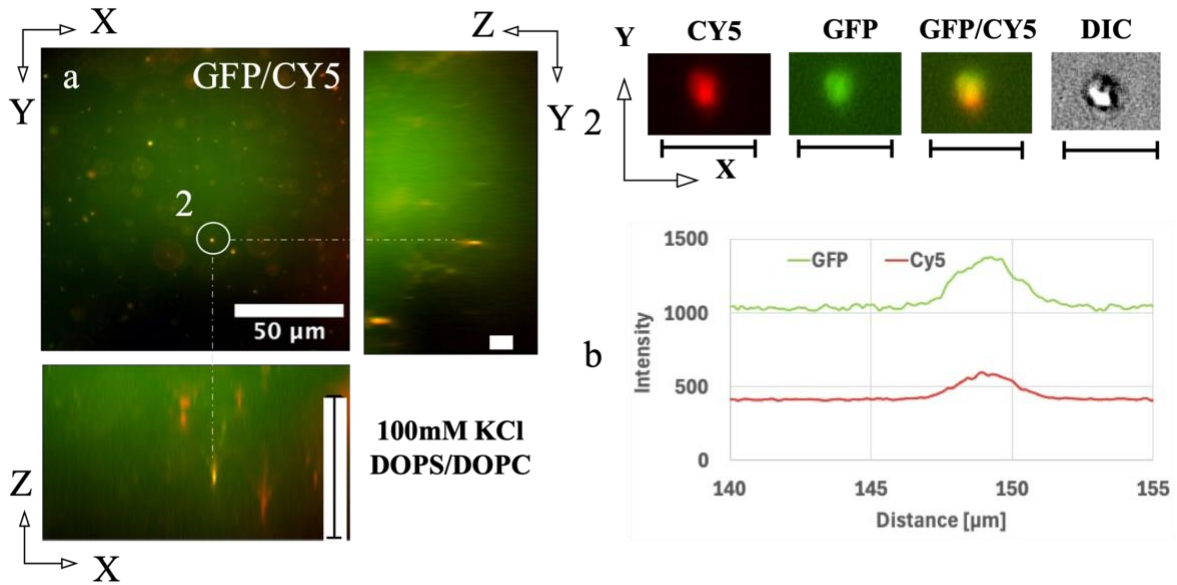


Figure 11. Fluorescent microscopy images of anionic liposomes and 4RL tau in 10mM KCl. The anionic liposomes made from 50% DOPS/ 49%DOPC/1% CY5.5 PE are visible in the Cy5 channel (RED) (Cy5.5 PE lipid - excitation/emission 683nm/703nm) and 4RL tau tagged with Alexa-488 (Alexa 488 excitation/emission: 488nm/496nm) are visible in the GFP channel (green). (a) A Z-stack image showing both GFP and Cy5 channels. The top left frame shows the X-Y section view at a chosen Z. The panels to the right show the Y-Z slice along the vertical dotted line marking the circled object 2. The bottom panel shows the X-Z section along the horizontal dotted line of object 2. (Scale bars correspond to 50 μ m in the X-Y, 200 μ m in X-Z and 20 μ m in Y-Z planes, respectively) (b) Detail view of particle 2: a anionic liposome-4RL tau complex. Top panel from left to right: magnified fluorescent (Cy5, GFP and GFP/Cy5 overlay) and DIC images of particle 2. Bottom panel: fluorescent intensity profiles of particle 2 in Cy5/GFP channels as a function of X. [*10 μ m scale bars*]

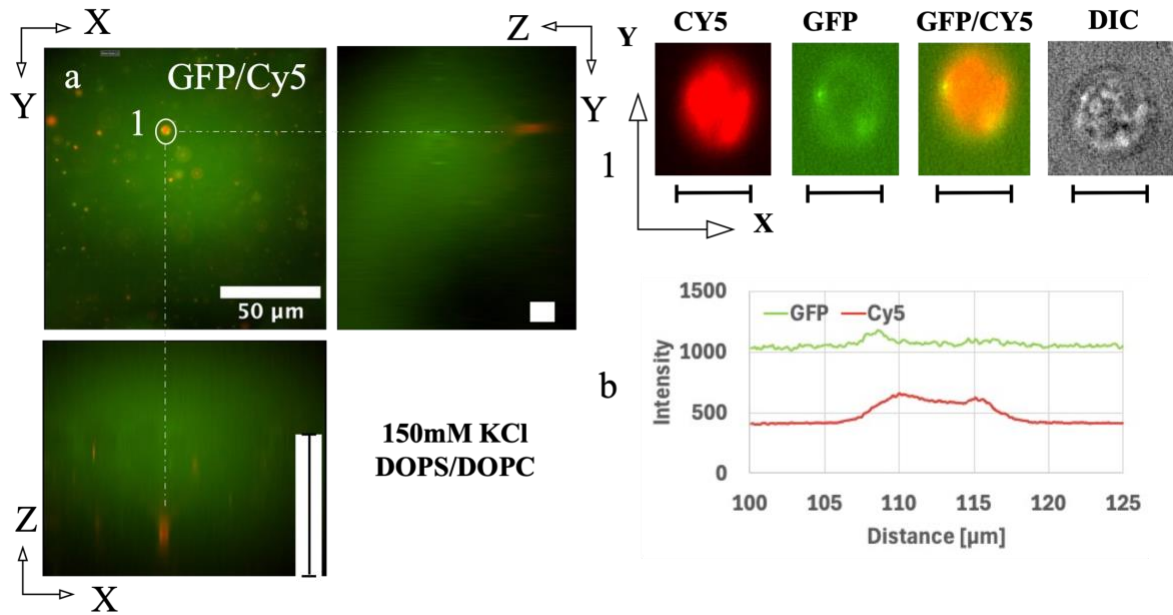


Figure 12. Fluorescent microscopy images of anionic liposomes and 4RL tau in 150mM KCl. The anionic liposomes made from 50% DOPS/ 49%DOPC/1% CY5.5 PE are visible in the Cy5 channel (RED) (Cy5.5 PE lipid - excitation/emission 683nm/703nm) and 4RL tau tagged with Alexa-488 (Alexa 488 excitation/emission: 488nm/496nm) are visible in the GFP channel (green). (a) A Z-stack image showing both GFP and Cy5 channels. The top left frame shows the X-Y section view at a chosen Z. The panels to the right show the Y-Z slice along the vertical dotted line marking the circled object 1. The bottom panel shows the X-Z section along the horizontal dotted line of object 1. (Scale bars correspond to 50 μ m in the X-Y, 200 μ m in X-Z and 20 μ m in Y-Z planes, respectively) (b) Detail view of particle 1: a giant anionic liposome-4RL tau complex. Top panel from left to right: magnified fluorescent (Cy5, GFP and GFP/Cy5 overlay) and DIC images of particle 1. Bottom panel: fluorescent intensity profiles of particle 1 in Cy5/GFP channels as a function of X. [10 μ m scale bars]

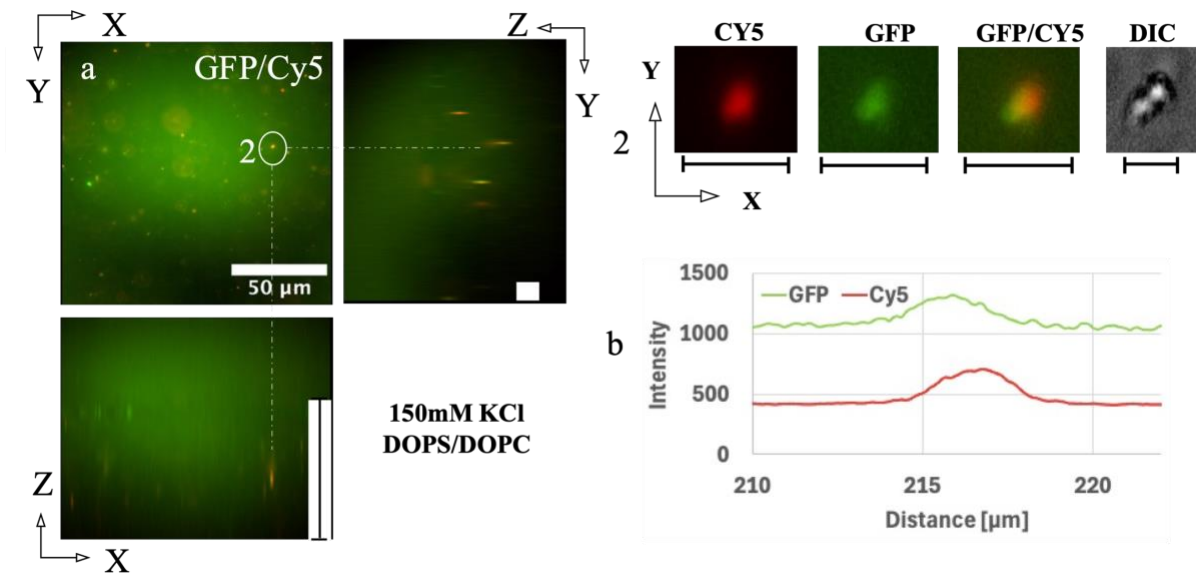


Figure 13. Fluorescent microscopy images of anionic liposomes and 4RL tau in 150mM KCl. The anionic liposomes made from 50% DOPS/ 49%DOPC/1% CY5.5 PE are visible in the Cy5 channel (RED) (Cy5.5 PE lipid - excitation/emission 683nm/703nm) and 4RL tau tagged with Alexa-488 (Alexa 488 excitation/emission: 488nm/496nm) are visible in the GFP channel (green). (a) A Z-stack image showing both GFP and Cy5 channels. The top left frame shows the X-Y section view at a chosen Z. The panels to the right show the Y-Z slice along the vertical dotted line marking the circled object 2. The bottom panel shows the X-Z section along the horizontal dotted line of object 2. (Scale bars correspond to 50μm in the X-Y, 200μm in X-Z and 20μm in Y-Z planes, respectively) (b) Detail view of particle 2: a anionic liposome-4RL tau complex. Top panel from left to right: magnified fluorescent (Cy5, GFP and GFP/Cy5 overlay) and DIC images of particle 2. Bottom panel: fluorescent intensity profiles of particle 2 in Cy5/GFP channels as a function of X. [$10\mu\text{m}$ scale bars]

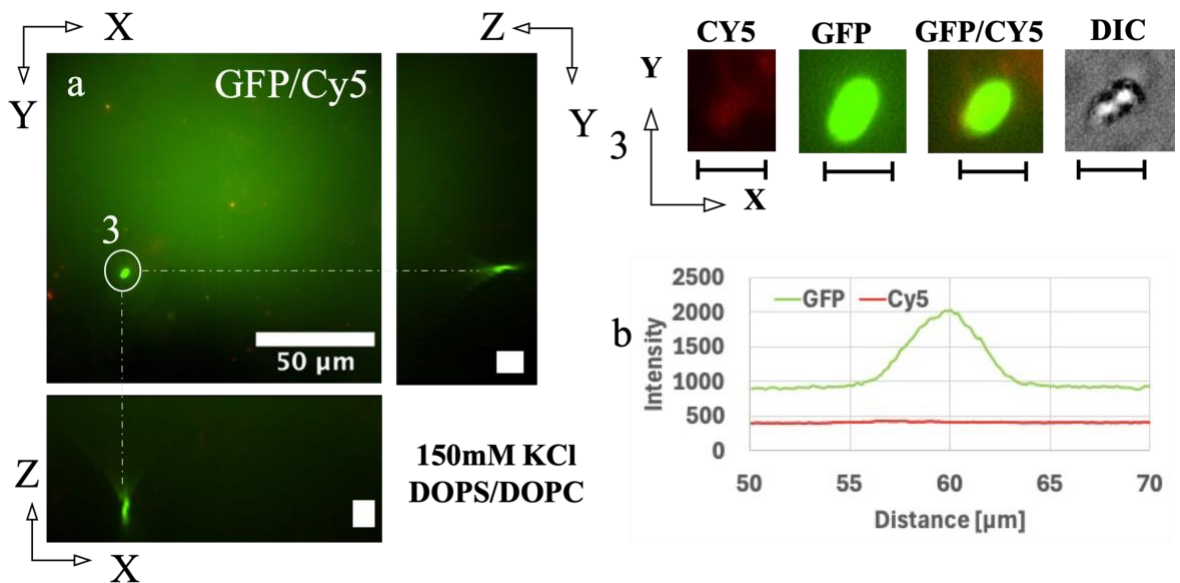


Figure 14. Fluorescent microscopy images of anionic liposomes and 4RL tau in 150mM KCl. The anionic liposomes made from 50% DOPS/ 49%DOPC/1% CY5.5 PE are visible in the Cy5 channel (RED) (Cy5.5 PE lipid - excitation/emission 683nm/703nm) and 4RL tau tagged with Alexa-488 (Alexa 488 excitation/emission: 488nm/496nm) are visible in the GFP channel (green). (a) A Z-stack image showing both GFP and Cy5 channels. The top left frame shows the X-Y section view at a chosen Z. The panels to the right show the Y-Z slice along the vertical dotted line marking the circled object 3. The bottom panel shows the X-Z section along the horizontal dotted line of object 3. (Scale bars correspond to 50 μ m in the X-Y, 200 μ m in X-Z and 20 μ m in Y-Z planes, respectively) (b) Detail view of particle 3: a tau coacervate with lipid assembly. Top panel from left to right: magnified fluorescent (Cy5, GFP and GFP/Cy5 overlay) and DIC images of particle 3. Bottom panel: fluorescent intensity profiles of particle 3 in Cy5/GFP channels as a function of X. [*10 μ m scale bars*]

IV. Conclusion

Intrinsically disordered protein tau, an overall positive polyampholyte, is a microtubule (MT)-associated protein localized to axons in vertebrate neurons. Tau regulates MT dynamic instability and aberrant tau-MT interactions is implicated in Alzheimer's and other neurodegenerative diseases. While there is incomplete understanding of the mechanisms driving neurodegenerative pathology, some evidence exists that aside from tubulin and MTs (tau's natural substrates) tau can interact with other anionic macromolecules including lipids. However, the extent and conditions of these interactions are not understood. Here, we investigated the structural implications of the electrostatic associations of full length human 4RL-tau with anionic liposomes containing either 1,2-dioleoyl-sn-glycero-3-phosphatidylserine (DOPS, charge = -1e) or 1,2-dioleoyl-sn-glycero-3-phosphatidylglycerol (DOPG, charge = -1e) mixed with zwitterionic 1,2-dioleoyl-sn-glycero-3-phosphatidylcholine (DOPC) to mimic anionic plasma membranes of axons where tau resides. Using differential interference contrast and fluorescence microscopy, we studied the phase behavior of mixtures of 4RL-tau and anionic liposomes (ALs) at low and high salt concentrations at lipid/tau molar charge ratio. At low ionic strengths with minimal charge screening, distinct phase separated states of AL-tau complexes coexisted with liquid-liquid phase separated tau self-coacervates due to the polyampholytic nature of tau. AL-tau complex morphologies included giant vesicles (uni- and multi-lamellar) with bound tau-membrane domains and assemblies of smaller liposomes bound together through Tau's cationic domains. The tau self-coacervates were observed to dissolve with increasing ionic strength approaching physiological 1:1 electrolyte concentration (100mM to 150 mM). In contrast, AL-tau complexes remain stable in the higher salt concentration conditions implying that the electrostatic interactions of

polyampholyte tau with anionic membranes is significantly stronger than electrostatic interactions stabilizing tau self-coacervates (i.e. where we find that only at low ionic strengths (conditions not found in axons) tau self-coacervates are stable).

The findings are consistent with the hypothesis that the overall positively charged tau may interact with anionic domains of the lumen facing lipid monolayer of the axon plasma membranes, through long-lived or transient robust interactions at physiologically relevant ionic strengths. For tau bound to MTs, the relevant cationic domains involved in interactions with negative lipid domains include the PRR and large sections of the C-terminal domain, which flank the MTBR region (i.e. where different fractions of tau bind MTs and negative membrane domains simultaneously). For free tau, the heavily cationic MTBR is also a site for tau-membrane interactions.

The anionic liposome-tau complexes described in this study may be referred to as tau-lipoplexes in analogy with lipoplexes consisting of cationic liposome-DNA complexes used in nucleic acid delivery applications.^{43,44} While the current study focused on elucidating phase separated structures on the optical micron scale, we expect that future small-angle X-ray scattering studies, both in bulk phases and dilute solutions similar to conditions in this study, will reveal a rich variety of distinct structures (lamellar, hexagonal, and cubic phases) on the nanometer and angstrom scales that have been observed for CL-nucleic acid lipoplexes.

References

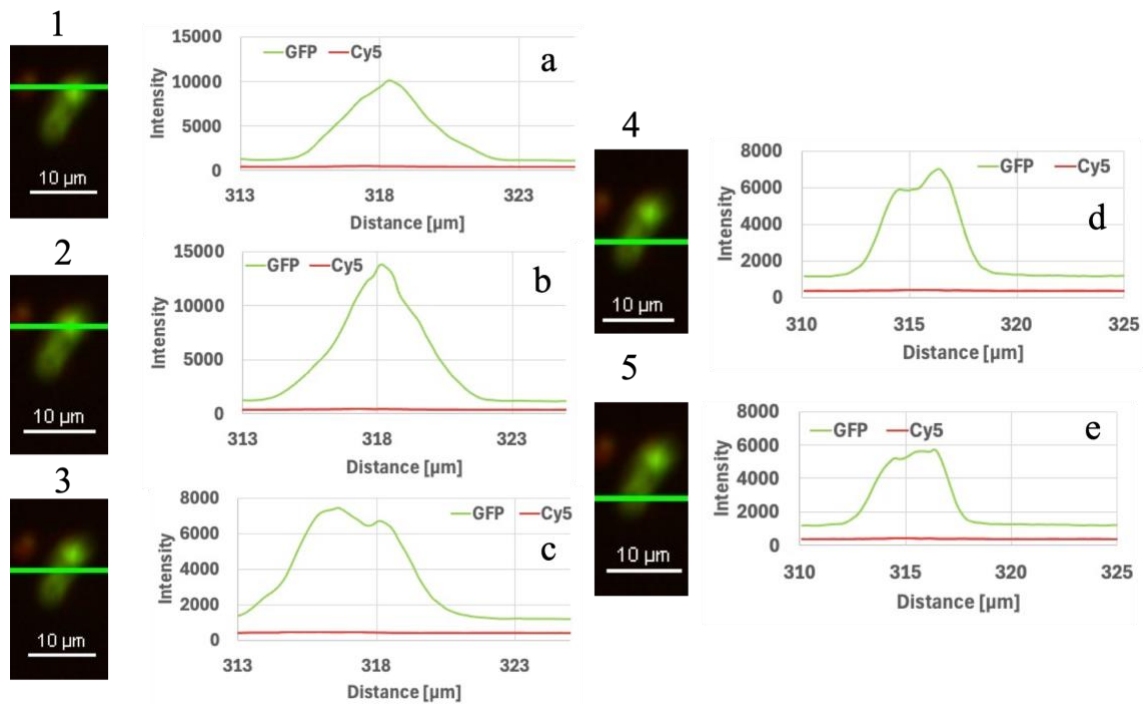
1. Himmler, A.; Drechsel, D.; Kirschner, M. W.; Martin, D. W., Jr. Tau consists of a set of proteins with repeated C-terminal microtubule-binding domains and variable N-terminal domains. *Mol. Cell Biol.* 1989, 9 (4), 1381–1388.
2. Lee, G.; Cowan, N.; Kirschner, M. The primary structure and heterogeneity of tau protein from mouse brain. *Science* 1988, 239 (4837), 285–288.
3. Butner, K. A.; Kirschner, M. W. Tau protein binds to microtubules through a flexible array of distributed weak sites. *J. Cell Biol.* 1991, 115 (3), 717–730.
4. Lee, G.; Neve, R. L.; Kosik, K. S. The microtubule binding domain of tau protein. *Neuron* 1989, 2 (6), 1615–1624.
5. Goode, B. L.; Feinstein, S. C. Identification of a novel microtubule binding and assembly domain in the developmentally regulated inter-repeat region of tau. *J. Cell Biol.* 1994, 124 (5), 769–782.
6. Kellogg, E. H.; Hejab, N. M.; Howes, S.; Northcote, P.; Miller, J. H.; Diaz, F.; Downing, K. H.; Nogales, E. Near-Atomic Model of Microtubule-Tau Interactions. *Science* 2018, 360 (6394), 1242–1246.
7. Charge taken from protein database
<https://www.uniprot.org/uniprotkb/Q6B856/entry>.
8. Amos, L. A.; Baker, T. S. The three-dimensional structure of tubulin protofilaments. *Nature* 1979, 279 (5714), 607–612.
9. Löwe, J.; Li, H.; Downing, K. H.; Nogales, E. Refined structure of alpha beta-tubulin at 3.5 Å resolution. *J. Mol. Biol.* 2001, 313 (5), 1045–1057.
10. Ojeda-Lopez, M. A.; et al. Transformation of taxol-stabilized microtubules into inverted tubulin tubules triggered by a tubulin conformation switch. *Nat. Mater.* 2014, 13 (2), 195–203.
11. Desai, A.; Mitchison, T. J. Microtubule polymerization dynamics. *Annu. Rev. Cell Dev. Biol.* 1997, 13, 83–117.
12. Pollard, T. D.; Earnshaw, W. C.; Lippincott-Schwartz, J. *Cell Biology*, 3rd Ed.; Saunders/Elsevier: Philadelphia, 2017.
13. Alushin, G. M.; et al. High-resolution microtubule structures reveal the structural transitions in alpha beta-tubulin upon GTP hydrolysis. *Cell* 2014, 157, 1117–1129.
14. Rice, L. M.; Montabana, E. A.; Agard, D. A. The lattice as allosteric effector: structural studies of alpha beta- and gamma-tubulin clarify the role of GTP in microtubule assembly. *Proc. Natl. Acad. Sci. U.S.A.* 2008, 105, 5378–5383.
15. Hyman, A. A.; Chretien, D.; Arnal, I.; Wade, R. H. Structural changes accompanying GTP hydrolysis in microtubules: information from a slowly hydrolyzable analogue guanylyl-(alpha,beta)-methylene-diphosphonate. *J. Cell Biol.* 1995, 128, 117–125.
16. Muller-Reichert, T.; Chretien, D.; Severin, F.; Hyman, A. A. Structural changes at microtubule ends accompanying GTP hydrolysis: information from a slowly hydrolyzable analogue of GTP, guanylyl (alpha,beta)-methylenediphosphonate. *Proc. Natl. Acad. Sci. U.S.A.* 1998, 95, 3661–3666.
17. Chretien, D.; Fuller, S. D.; Karsenti, E. Structure of growing microtubule ends: two-dimensional sheets close into tubes at variable rates. *J. Cell Biol.* 1995, 129, 1311–1328.

18. Morris, M.; Maeda, S.; Vossel, K.; Mucke, L. The many faces of tau. *Neuron* 2011, 70 (3), 410–426. doi:10.1016/j.neuron.2011.04.009.
19. Human Microtubule-Associated-Protein Tau Regulates the Number of Protofilaments in Microtubules: A Synchrotron X-ray Scattering Study”, by M.C. Choi, U. Raviv, H. Miller, M.R. Gaylord, E. Kiris, D. Ventimiglia, D. Needleman, M.W. Kim, L. Wilson, S.C. Feinstein and C.R. Safinya, *Biophysical Journal* 29 (2), 519-527, 2009)
20. Chung, P. J.; Choi, M. C.; Miller, H. P.; Feinstein, H. E.; Raviv, U.; Li, Y.; Wilson, L.; Feinstein, S. L.; Safinya, C. R.: Direct force measurements reveal that protein Tau confers short-range attractions and isoform-dependent steric stabilization to microtubules. *Proc. Natl. Acad. Sci. U. S. A. (PNAS Plus)* 2015, 112, E6416-E6425.
21. Chung, P. J.; Song, C.; Miller, H. P.; Li, Y.; Choi, M. C.; Wilson, L.; Feinstein, S. C.; Safinya, C. R.: Tau mediates microtubule bundle architectures mimicking fascicles of microtubules found in the axon initial segment. *Nature Communications* 2016, 7, 12278.
22. Kohl, P. A.; Song, C.; Fletcher, B. J.; Best, R. L.; Tchounwou, C.; Arceo, X. G.; Chung, P. J.; Miller, H. P.; Wilson, L.; Choi, M. C.; Li, Y.; Feinstein, S. C.; Safinya, C. R.: Complexes of tubulin oligomers and tau form a viscoelastic intervening network cross-bridging microtubules into bundles. *Nature Communications* 2024, 15, 2362.
23. Drechsel, D. N.; Hyman, A. A.; Cobb, M. H.; Kirschner, M. W. Modulation of the dynamic instability of tubulin assembly by the microtubule-associated protein tau. *Mol. Biol. Cell* 1992, 3 (10), 1141–1154.
24. Gustke, N.; Trinczek, B.; Biernat, J.; Mandelkow, E. M.; Mandelkow, E. Domains of tau protein and interactions with microtubules. *Biochemistry* 1994, 33 (32), 9511–9522.
25. Panda, D.; Goode, B. L.; Feinstein, S. C.; Wilson, L. Kinetic stabilization of microtubule dynamics at steady state by tau and microtubule-binding domains of tau. *Biochemistry* 1995, 34, 11117–11127.
26. Trinczek, B.; Biernat, J.; Baumann, K.; Mandelkow, E. M.; Mandelkow, E. Domains of tau protein, differential phosphorylation, and dynamic instability of microtubules. *Mol. Biol. Cell* 1995, 6, 1887–1902.
27. Panda, D.; Samuel, J. C.; Massie, M.; Feinstein, S. C.; Wilson, L. Differential regulation of microtubule dynamics by three- and four-repeat tau: Implications for the onset of neurodegenerative disease. *Proc. Natl. Acad. Sci. U.S.A.* 2003, 100 (16), 9548–9553.
28. Cleveland, D. W.; Hwo, S. Y.; Kirschner, M. W. Purification of tau, a microtubule-associated protein that induces assembly of microtubules from purified tubulin. *J. Mol. Biol.* 1977, 116, 207–225.
29. Selkoe, D. J. The Molecular Pathology of Alzheimer's Disease. *Neuron* 1991, 6 (4), 487-498. DOI: 10.1016/0896-6273(91)90052-2. PMID: 1673054.
30. Kosik, K. S.; Joachim, C. L.; Selkoe, D. J. Microtubule-associated protein tau (tau) is a major antigenic component of paired helical filaments in Alzheimer disease. *Proc. Natl. Acad. Sci. U.S.A.* 1986, 83, 4044–4048.
31. Huang, Y.; Mucke, L. Alzheimer mechanisms and therapeutic strategies. *Cell* 2012, 148 (6), 1204–1222.

32. Li, X. H.; Rhoades, E. Heterogeneous Tau-Tubulin Complexes Accelerate Microtubule Polymerization. *Biophys. J.* 2017, *112* (12), 2567–2574.
33. Tettamanti, G.; Goracci, G., Eds. Handbook of Neurochemistry and Molecular Neurobiology, Neural Lipids; Springer: 2009.
34. Brandt, R.; Léger, J.; Lee, G. Interaction of Tau with the Neural Plasma Membrane Mediated by Tau's Amino-Terminal Projection Domain. *J. Cell Biol.* 1995, *131* (5), 1327–1340. DOI: 10.1083/jcb.131.5.1327. PMID: 8522593; PMCID: PMC2120645.
35. Najafi, S.; Lin, Y.; Longhini, A. P.; Zhang, X.; Delaney, K. T.; Kosik, K. S.; Fredrickson, G. H.; Shea, J. E.; Han, S. Liquid-liquid phase separation of Tau by self and complex coacervation. *Protein Sci.* 2021, *30* (7), 1393–1407.
36. Kanaan, N.; Hamel, C.; Grabinski, T.; Combs, B. Liquid-liquid phase separation induces pathogenic tau conformations in vitro. *Nat. Commun.* 2020, *11*, 10.1038/s41467-020-16580-3.
37. Ambadipudi, S.; Biernat, J.; Riedel, D.; Mandelkow, E.; Zweckstetter, M. Liquid-liquid phase separation of the microtubule-binding repeats of the Alzheimer-related protein Tau. *Nat. Commun.* 2017, *8* (1), 275. doi:10.1038/s41467-017-00480-0.
38. Wegmann, S.; Eftekharzadeh, B.; Tepper, K.; et al. Tau protein liquid-liquid phase separation can initiate tau aggregation. *EMBO J.* 2018, *37* (7), e98049.
39. Koltover, I.; Radler, J. O.; Safinya, C. R. Membrane mediated attraction and ordered aggregation of colloidal particles bound to giant phospholipid vesicles. *Phys. Rev. Lett.* 1999, *82*, 1991–1994.
40. Walker, S. A.; Kennedy, M. T.; Zasadzinski, J. A. Encapsulation of bilayer vesicles by self-assembly. *Nature* 1997, *387* (6628), 61–64. doi:10.1038/387061a0.
41. Kisak, E. T.; Coldren, B.; Evans, C. A.; Boyer, C.; Zasadzinski, J. A. The vesosome - a multicompartement drug delivery vehicle. *Curr. Med. Chem.* 2004, *11* (2), 199–219. doi:10.2174/0929867043456197.
42. Lipids purchased and sketches obtained from Avanti Lipids catalog: <https://avantilipids.com>.
43. Felgner, P. L.; Gadek, T. R.; Holm, M.; Roman, R.; Chan, H. W.; Wenz, M.; Northrop, J. P.; Ringold, G. M.; Danielsen, M.: Lipofection: a highly efficient, lipid-mediated DNA-transfection procedure. *Proc. Natl. Acad. Sci. U. S. A.* 1987, *84*, 7413-7417.
44. Ewert, K. K.; Scodeller, P.; Simón-Gracia, L.; Steffes, V. M.; Wonder, E. A.; Teesalu, T.; Safinya, C. R.: Cationic Liposomes as Vectors for Nucleic Acid and Hydrophobic Drug Therapeutics. *Pharmaceutics* 2021, *13*, 1365.
45. Safinya, C. R.; Ewert, K. K.; Majzoub, R. N.; Leal, C.: Cationic liposome-nucleic acid complexes for gene delivery and gene silencing. *New J. Chem.* 2014, *38*, 5164-5172.
46. Ewert, K.; Slack, N. L.; Ahmad, A.; Evans, H. M.; Lin, A. J.; Samuel, C. E.; Safinya, C. R. Cationic lipid-DNA complexes for gene therapy: Understanding the relationship between complex structure and gene delivery pathways at the molecular level. *Curr. Med. Chem.* 2004, *11*, 133-149.
47. Ewert, K.; Ahmad, A.; Evans, H. M.; Schmidt, H. W.; Safinya, C. R. Efficient synthesis and cell-transfection properties of a new multivalent cationic lipid for nonviral gene delivery. *J. Med. Chem.* 2002, *45*, 5023-5029.

48. Rädler, J. O.; Koltover, I.; Salditt, T.; Safinya, C. R. Structure of DNA-cationic liposome complexes: DNA intercalation in multilamellar membranes in distinct interhelical packing regimes. *Science* 1997, *275*, 810-814.
49. Lin, A. J.; Slack, N. L.; Ahmad, A.; George, C. X.; Samuel, C. E.; Safinya, C. R. Three-dimensional imaging of lipid gene-carriers: Membrane charge density controls universal transfection behavior in lamellar cationic liposome-DNA complexes. *Biophys. J.* 2003, *84*, 3307-3316.
50. Ahmad, A.; Evans, H. M.; Ewert, K.; George, C. X.; Samuel, C. E.; Safinya, C. R. New multivalent cationic lipids reveal bell curve for transfection efficiency versus membrane charge density: Lipid - DNA complexes for gene delivery. *J. Gene. Med.* 2005, *7*, 739-748.
51. Majzoub, R. N.; Ewert, K. K.; Jacovetty, E. L.; Carragher, B.; Potter, C. S.; Li, Y.; Safinya, C. R.: Patterned Threadlike Micelles and DNA-Tethered Nanoparticles: A Structural Study of PEGylated Cationic Liposome–DNA Assemblies. *Langmuir* 2015, *31*, 7073-7083. PMID: PMC4554524.
52. Koltover, I.; Salditt, T.; Rädler, J. O.; Safinya, C. R. An inverted hexagonal phase of cationic liposome-DNA complexes related to DNA release and delivery. *Science* 1998, *281*, 78-81.
53. Ewert, K. K.; Evans, H. M.; Zidovska, A.; Boussein, N. F.; Ahmad, A.; Safinya, C. R. A columnar phase of dendritic lipid-based cationic liposome-DNA complexes for gene delivery: Hexagonally ordered cylindrical micelles embedded in a DNA honeycomb lattice. *J. Am. Chem. Soc.* 2006, *128*, 3998-4006.
54. Ewert, K. K.; Evans, H. M.; Boussein, N. F.; Safinya, C. R. Dendritic cationic lipids with highly charged headgroups for efficient gene delivery. *Bioconjugate Chem.* 2006, *17*, 877-888.
55. Leal, C. I.; Boussein, N. F.; Ewert, K. K.; Safinya, C. R. Highly Efficient Gene Silencing Activity of siRNA Embedded in a Nanostructured Gyroid Cubic Lipid Matrix. *J. Am. Chem. Soc.* 2010, *132*, 16841-16847. DOI:
56. Leal, C.; Ewert, K. K.; Shirazi, R. S.; Boussein, N. F.; Safinya, C. R. Nanogyroids Incorporating Multivalent Lipids: Enhanced Membrane Charge Density and Pore Forming Ability for Gene Silencing. *Langmuir* 2011, *27*, 7691-7697.
57. Yanez Arteta, M.; Kjellman, T.; Bartesaghi, S.; Wallin, S.; Wu, X.; Kvist, A. J.; Dabkowska, A.; Székely, N.; Radulescu, A.; Bergenholtz, J.; Lindfors, L.: Successful reprogramming of cellular protein production through mRNA delivered by functionalized lipid nanoparticles. *Proc. Natl. Acad. Sci. U. S. A.* 2018, *115*, E3351-E3360. DOI: 10.1073/pnas.1720542115.
58. Philipp, J.; et al. pH-dependent structural transitions in cationic ionizable lipid mesophases are critical for lipid nanoparticle function. *Proc. Natl. Acad. Sci. U. S. A.* 2023, *120* e2310491120

Appendix



Appendix Figure 1. Coacervate with hints of lipid assembly produced in mixture of anionic liposomes (50% DOPS/ 49%DOPC/1% CY5.5 PE) and 4RL tau tagged with Alexa-488 in 150mM KCl. (1-5) Slice taken of coacervate of merged CY5/GFP channel. (Cy5.5 PE lipid - excitation/emission 683nm/703nm) (Alexa 488 excitation/emission: 488nm/496nm). (a-e) 3D intensity maps taken at slice shown on particle.